# ASSESSMENT OF FLUORESCENTLY-LABELED GOLD NANOPARTICLES IN MICE AS A CONTRAST AGENT FOR MICRO-COMPUTED TOMOGRAPHY AND OPTICAL PROJECTION TOMOGRAPHY

by

Stevo Kozomara

A THESIS SUBMITTED IN PARTIAL FULFILLMENT OF

THE REQUIREMENTS FOR THE DEGREE OF

Master of Science

in

THE FACULTY OF GRADUATE AND POSTDOCTORAL STUDIES

(Craniofacial Sciences)

THE UNIVERSITY OF BRITISH COLUMBIA

(Vancouver)

May 2019

The following individuals certify that they have read, and recommend to the Faculty of Graduate and Postdoctoral Studies for acceptance, the dissertation entitled:

ASSESSMENT OF FLUORESCENTLY-LABELED GOLD NANOPARTICLES IN MICE AS A CONTRAST AGENT FOR MICRO-COMPUTED TOMOGRAPHY AND OPTICAL PROJECTION TOMOGRAPHY

submitted by Dr. Stevo Kozomara in partial fulfillment of the requirements for

the degree of Master of Science

in Craniofacial Science

**Examining Committee:**

Dr. Nancy L. Ford – Faculty of Dentistry
Supervisor

Dr. Edward E. Putnins – Faculty of Dentistry
Supervisory Committee Member

Dr. Clive R. Roberts – Faculty of Dentistry
Supervisory Committee Member

Dr. Siddharth Vora – Faculty of Dentistry
Additional Examiner

## Abstract

**Objectives**: Contrast agents are required to be able to view and differentiate tissues in 3-D computed tomography (CT) due to similarities in density. Pre-clinical contrast agents used for radiology are not visible when viewed histologically, and visa versa. Identifying a single agent that is visible in both x-ray and optical imaging, would ensure that the target tissues can be easily identified and correlated in both images, without the need of additional staining techniques. Here we present an approach for imaging the murine cardiovascular system and organs, and melanoma tumours using micro-computed tomography (micro-CT) and optical projection tomography (OPT), using fluorescently-labeled gold nanoparticles.

**Materials and Methods**: A 1% agarose phantom was used with 2 µl of the Cy3 fluorescently-labeled gold nanoparticles deposited in the block, and imaged with micro-CT and OPT. *In vivo* systemic testing involved tail vein intravascular injections into mice using Cy3 fluorescently-coated gold nanorods. These mice were subjected to micro-CT scans, both before and after contrast injection. Once euthanized, the heart, liver and kidneys were excised, scanned using the higher resolution specimen micro-CT scanner, then prepared, and visualized under OPT using filtered UV light at 545-610nm. Localized *in vivo* testing was performed using B16F10 cells to induce tumour growth in the right hind legs of mice. Cy3 fluorescently-coated gold nanorods were injected directly into the tumours prior to imaging. The mice were scanned with *in vivo* micro-CT for pre- and post-contrast scans. Once euthanized, the hind leg was dissected and scanned with a specimen micro-CT at a higher resolution. The dissected hind legs were prepared and visualized under OPT using filtered UV light at 545-610 nm.

**Results**: Using the agarose phantom, the gold nanoparticles were visible under both micro-CT and OPT, with co-localization between images. With the *in vivo* systemic testing, the nanoparticles

were not visible. The *in vivo* localized tumour study showed the distribution of the gold nanoparticles within the tumours, allowing for visualization under micro-CT. OPT imaging was successful and co-localized to micro-CT.

**Conclusions**: Cy3 fluorescently-labeled gold nanorods injected into murine melanoma tumours can be visualized under micro-CT imaging, and co-localized to OPT.

## Lay Summary

This research was done to determine if fluorescently-labeled gold nanoparticles could be visualized under both micro-computed tomography (micro-CT) and optical projection tomography (OPT). Gold as a heavy metal should be visible under micro-CT, but without fluorescent-labeling, gold would not be visible under light microscopy (OPT). To be able to see structures within samples under microscopy, the samples need to be processed and stained, which could affect the results and requires additional time and effort. Using fluorescently-labeled gold nanoparticles may allow for visualization using both micro-CT and OPT. To assess this hypothesis, we first injected fluorescently-labeled gold nanoparticles into an agarose block and visualized using micro-CT and OPT, matching the two images. Using *in vivo* imaging, we assessed if these same nanoparticles could be injected into the vascular system of mice to visualize them systemically. Using tumour-bearing mice, we injected the tumours directly with a localized dose of fluorescently-labeled gold nanoparticles.

## Preface

This research was done and written by the author, under the supervision of Dr. Nancy Ford. Ethics approval (A14-0125) was obtained prior to commencing with the small animal research. The culturing of the murine melanoma cells, in addition to providing assistance and guidance in usage of the micro-CT and OPT scanners, was done by Dr. Guobin Sun. The assessment of the results was done by the author and Dr. Ford. Part of this dissertation is planned for publication. At the time of writing, a portion of this research has been accepted for oral presentation at the 2019 SPIE Medical Imaging Conference, held in San Diego, California, USA, in addition to being published in Medical Imaging 2019: Biomedical Applications in Molecular, Structural, and Functional Imaging. (1)

## Table of Contents

Abstract……..…….iii

Lay Summary……..…..……..v

Preface ……vi

Table of Contents……..……vii

List of Tables …….....x

List of Figures…….xi

List of Abbreviations …….xii

Acknowledgements……...xiv

Dedication…….….xv

Charter 1: Introduction…….1

1.1 Importance of Pre-Clinical Research……...1

1.2 Small Animal Imaging ...……1

1.2.1 Pre-Clinical Micro-Computed Tomography……3

1.2.2 Specimen Micro-CT Scanners……...…..4

1.2.3 *In Vivo* Micro-CT Scanners……...……..5

1.3 Current Pre-Clinical Contrast Agents……...6

1.3.1 Gold Nanoparticles as Pre-Clinical Contrast Agents……8

1.4 Tumour Physiology and Imaging……...10

1.5 Histology as the "Gold Standard"……...11

1.6 Optical Projection Tomography…….12

1.7 Rationale…..……...13

Chapter 2: Experimental Methods……..15

2.1 Overview of Research Project……15

2.2 Nanoparticles……..16

2.3 Imaging Equipment……17

2.3.1 *In Vivo* Micro-Computed Tomography Scanner…….17

2.3.2 Specimen Micro-CT Scanner…….19

2.3.3 Optical Projection Tomography…….20

2.4 Agarose Phantom Experiments……..22

2.5 *In Vivo* Experiments……...23

2.5.1 Systemic Injections……23

2.5.2 Murine Melanoma Cell Culturing……..28

2.5.3 *In Vivo* Tumour Injections……..29

2.6 Data Analysis…….32

2.6.1 Tumour Measurements……...32

Chapter 3: Results……..34

3.1 Agarose Phantom……...34

3.2 *In Vivo* Systemic Injections……35

3.3 *In Vivo* Tumour Injections……..39

Chapter 4: Discussion…….48

4.1 Agarose Phantom……...48

4.2 *In Vivo* Systemic Injection……..49

4.3 *In Vivo* Tumour Injection……...50

4.4 Targeted Delivery of Nanoparticles……...54

Chapter 5: Conclusions and Future Directions……...57

5.1 Conclusions……57

5.2 Future Directions……58

Bibliography……..60

## List of Tables

Table 1. Hounsfield scale of common tissues and substances…….3

Table 2. Concentrations of Nanopartz® fluorescently-labeled gold nanorods …….17

Table 3. Imaging protocols for *in vivo* micro-CT……..19

Table 4. *In vivo* systemic injection parameters……..26

Table 5. Mouse tumour features at pre-contrast injection (tumours > $1cm^3$ as image-based tumour volume……...41

Table 6. Mouse tumour features at pre-contrast injection (tumours ≤ $1cm^3$ as image-based tumour volume)……..41

## List of Figures

Figure 1. Comparison of 50 and 250 OD Nanopartz® gold nanorods ……..16

Figure 2. TriFoil eXplore CT 120 *in vivo* micro-CT scanner……18

Figure 3. Scanco Medical µCT100 specimen scanner……...20

Figure 4. Bioptonics OPT scanner 3001M ……21

Figure 5. Sample in agarose block (arrow) adhered to mount, positioned above cuvette …….23

Figure 6. Mouse under inhaled anesthesia on micro-CT scanner bed……...24

Figure 7. Anesthetized mouse ready for tail vein injection (tail vein is visible) ……...25

Figure 8. Co-localization between OPT (left) and high-resolution micro-CT (right) ……...34

Figure 9. OPT images of Mouse #1 after tail vein injection of 200 µl of 50 OD Nanopartz® gold nanorods (from left: heart, kidney and liver)…….35

Figure 10. Images of micro-CT scan of Mouse #3 at 50 microns after tail vein injection of 200 µl of 250 OD Nanopartz® gold nanorods……..37

Figure 11. Images of micro-CT scan of Mouse #3 at 50 microns after tail vein injection of 200 µl of 250 OD Nanopartz® gold nanorods. The dots around the midsection are indicative of metal particles found in mouse feed ……38

Figure 12. OPT images of Mouse #3 after tail vein injection of 200 µl of 250 OD Nanopartz® gold nanorods (from left: heart, kidney and liver)…….38

Figure 13. Images showing the Region of Interest function, outlining the visualized tumour post-contrast injection, for *in vivo* micro-CT scan at 50 microns resolution. Left image is single slice through tumour with margins outlined, and right image is 3D region of interest containing the tumour, for Mouse #10, 12 and 8 respectively ……..42

Figure 14. Images of gold nanorods providing contrast for *in vivo* micro-CT scan at 50 microns resolution. Left image is pre-contrast and right image is post contrast injection of 20 µl of gold nanorod solution, of Mouse #10, 12 and 8 respectively. Arrows point to contrast ……...45

Figure 15. Image of 20 µl injection of gold nanorods providing for *in vivo* micro-CT scan of Mouse #10, 12, and 8 respectively at 50 microns resolution ……46

Figure 16. Image of tumour post-injection of 20 µl of gold nanorods providing contrast for specimen micro-CT scan at 10 microns resolution (LEFT), and OPT scan of dissected right hindleg (RIGHT). The sample was scanned at an exposure of 600ms, and UV light filter of TXR 560/40nm, 610nm used (RIGHT). Mouse #10, 12, and 8 respectively ……...47

## List of Abbreviations

2D: two dimensions

3D: three dimensions

BABB: benzyl alcohol and benzyl benzoate

CT: computed tomography

DNA: deoxyribonucleic acid

ECG: electrocardiography

EPR: enhanced permeability and retention

g: gram

Gy: gray unit of absorbed dose

HIV: human immunodeficiency virus

HU: Hounsfield unit

IM: intramuscular

IP: intraperitoneal

keV: kilo electron volt

kg: kilogram

kVp: kilovoltage peak

Micro-CT : micro-computed tomography

µl: micro-litre

mA: milliamperes

mg: milligram

ml: millilitre

MRI: magnetic resonance imaging

MRM: magnetic resonance microscopy

ms: milliseconds

nm: nanometre

OD: optical density

OPT: optical projection tomography

PBS: phosphate buffered saline

PC: personal computer

PEG: polyethylene glycol

PET: positron emission tomography

RNA: ribonucleic acid

RPM: revolutions per minute

SPECT: single photon emission computed tomography

SPIE: Society of Photographic Instrumentation Engineers

TAT: transactivator of transcription

UV: ultraviolet

## Acknowledgements

I offer my enduring gratitude to the periodontics faculty, staff and my fellow residents at UBC, who have inspired me to continue my work in this field. I owe particular thanks to my supervisor, Dr. Nancy L. Ford, whose enthusiasm, motivation and guidance helped me achieve my goal. Thank you for taking a chance on me and allowing me the honour to work with you. Your valuable time and input in the writing of this document was especially appreciated.

I would like to thank my committee members, Dr. E. Putnins and Dr. C. Roberts for their insightful comments and willingness to offer advice and encouragement. They were always available to meet and discuss and presented valuable advice throughout this journey.

I would also like to thank Dr. Guobin Sun for his assistance in the culturing of the melanoma cells, and for his patience in teaching me how to use the imaging software and associated lab protocols. He frequently took time out of his day to assist me when needed, and I can't thank him enough.

A special thank you is also extended to the Natural Sciences and Engineering Research Council (NSERC) for their generous grant, making this research possible.

Last, but not least, I would like to thank my wife Natasha, whose love and incredible support, made this all possible. You always encouraged me to follow my dreams, and you've literally gone to the edges of the globe and back with me. You've blessed me with two beautiful children and selflessly supported me throughout this entire journey. I want you to know, that I could not have done this without you!

## Dedication

To my late parents, Nikola and Milka,

Even though our time together was cut short, you raised me to be the man that I am today. A loving husband, and a caring father. I miss you both tremendously, and I hope I've made you both proud.

Love you always and forever.

# Chapter 1: Introduction

## 1.1 Importance of Pre-Clinical Research

Preclinical animal research is integral to pharmaceutical sciences and allows for the testing of novel drugs and modalities, prior to their introduction to clinical trials, in controlled animal settings. (2) Not only is this a good "first start" for research from an economic standpoint, but it also limits the pharmacological risks associated with phased clinical trials on human beings. The risk to human beings is obvious but what is sometimes less evident are the associated costs involved in drug development. According to the Tufts Center for the Study of Drug Development (CSDD) from 2014, which provides a regular assessment of drug development costs, the average cost to bring a new approved drug to market is $2.558 billion dollars (using 2013 US dollar estimates). (3) However, more staggering is the fact that only 5% of oncology drugs developed for clinical treatment, actually reach their intended target. (4) This further compounds the financial issue when one is reminded that while the cost to bring a drug to market is high, at that point, costs can be recovered through expected sales. Yet the preclinical costs for drug development cost on average $1.5 billion, which is money lost to a product that will never reach clinical phase trials. (3) Regardless, the associated benefits of preclinical research can not be overstated, especially when one considers the use of preclinical imaging and its betterment to the process.

## 1.2 Small Animal Imaging

The use of rodent and small animal imaging allows for the ability to study human disease processes in a longitudinal manner. In addition to micro-computed tomography, there exists micro-magnetic resonance imaging (micro-MRI), micro-magnetic resonance microscopy (micro-MRM), micro-positron emission tomography (micro-PET), high-resolution single photon

emission computed tomography (SPECT), and optical imaging, to name a few. (2) There are clearly several advantages to being able to utilize small animal imaging. Apart from requiring fewer animals as needed in biodistribution studies, small animal imaging also limits the need for more animals by offering a "replacement" option, as it were. The ability to utilize a non-invasive imaging modality, to view the internal organs, pathology and development, is a clear advantage. (5) Additionally, while the imaging modality itself is non-invasive, the animals are often anesthetized during the procedure, which limits their suffering by replacing procedures such as blood samples or more invasive investigative techniques. (2)

There will always be a desire for better and improved imaging for small animals in preclinical research. By developing targeted preclinical imaging modalities (for example, the use of contrast agents in computed tomography and peripheral vascular angiography), we will be able to better visualize the disease process being studied and utilize the developing therapy to treat said disease. Furthermore, the ability to create targeting medications (for instance, oncology drugs specifically targeting diseased vs. healthy tissues), and to study them under the guidance of preclinical small animal imaging, would allow for safer and ideally less costly, phased clinical trials in human beings. Lastly, small animal imaging also allows for fewer animals being needed for preclinical research as multiple imaging studies can be performed on animals throughout an experiment, prior to reaching experimental endpoint. Without the use of imaging techniques, an animal would potentially need to be euthanized and invasively investigated, thereby preventing the experiment from continuing further. With small animal imaging, the use of a non-invasive investigative tool precludes the early need of animal sacrifice, thereby reducing the number of animals needed for study.

### 1.2.1 Pre-Clinical Micro-Computed Tomography

In small animal imaging for pre-clinical research, micro-computed tomography (micro-CT) is often the imaging modality of choice due to its high-spatial resolution, excellent sensitivity to both bone and lung, relatively short scan time and cost-effectiveness. (5) By using the Hounsfield scale, a quantitative measurement can be used for describing the radiodensity of objects as seen in the scan. Commonly, the parameters are set within the machine and software so as to give air a value of -1000 HU and water a value of 0 HU. Table 1 provides the range of HU of commonly seen in tissues and substances, in a radiographic image.

Table 1. Hounsfield scale of common tissues and substances (6–8)

| **Substance** | **Hounsfield Units** |
|---|---|
| Air | -1000 |
| Water | 0 |
| Bone, cancellous | 300-400 |
| Bone, cortical | 1800-1900 |
| Muscle | 34-55 |
| Iodine (at 50 mg/ml) | 1600 |
| Gold | 2900 |

The true benefit of micro-CT is found within its name: the ability to provide resolution at the micron level. The use of other systems such as micro-MRI, and SPECT are arguably more beneficial in acquiring functional images, however, with a lower resolution. (5) Micro-MRI for example, is similar in its approach to micro-CT, with being able to provide higher resolution

images compared to standard MRI imaging. However, the two differ in that MRI is better suited at imaging soft tissue structures while also using non-ionizing radiation. Drawbacks to micro-MRI include relatively low sensitivity and long acquisition times, and the initial costs associated with the equipment are very high. (9,10) SPECT imaging utilizes radioisotope decay by detecting gamma-radiation from injected radioisotopes (probes). The benefit to using SPECT imaging is that multiple probes can be detected simultaneously. One clear disadvantage to this form of imaging is the required injection of a radioactive substance, in addition to the low resolution provided (1-2 mm) compared to other imaging modalities. (9,10)

### 1.2.2 Specimen Micro-CT Scanners

Further differentiation of micro-CT scanners includes both *in vivo* and specimen micro-CT scanners. Specimen scanners are often used when very high resolutions are required, thereby extending scan times tremendously. These are often reserved for small objects, excised tissues or intact rodents post-mortem. When discussing the type of scanning being employed, virtually all specimen scanners operate as rotational bed scans, using step and shoot image acquisition, whereas most *in vivo* scanners employ rotational gantry. (2) The voxel sizes that can be achieved using a typical commercially available specimen scanner typically ranges between 5.0 μm – 200 μm, however using the smallest voxel size (which also means it is higher in resolution) inevitably means that the scan time will be considerably longer. As the scan times increase, so too does the dose to the animal or sample, which is why the use of a specimen scanner is reserved to either euthanized whole animals, or dissected organs. In addition, the size of the output data set is directly proportional to the resolution. Finally, a limitation of the specimen scanning process is the size of the specimen being studied. As sample sizes increase, if the scanning resolution isn't adjusted

accordingly, the scan time and the resulting data set may be very large. As a result, a compromise is often made by increasing the voxel size to achieve adequate detail yet keeping the scan times and data sets manageable. (11)

### 1.2.3 *In Vivo* Micro-CT Scanners

*In vivo* scanning is performed on live, anesthetized small animals, and often with shorter scan durations and lower resolution (and larger voxel size). These scanners often allow for quantitative measurements of anatomy, tumours, blood vessels and organs. Using the example of the *in vivo* scanner currently available at The Centre for High-Throughput Phenogenomics at The University of British Columbia, additional benefits include high energy (70-120 kVp), high-throughput (1-15 minutes per scan), high resolution (25-100 μm), large fields of view (85 mm in diameter, 55 mm to 275 mm in length), and low dose *in vivo* imaging for rodents (mice and rats). It needs to be stated that a mouse will have a respiratory rate on average, of 80 – 230 breaths per minute, and will also have an average heart rate of 310 – 840 beats per minute. This could potentially become problematic during an *in vivo* scan as the movement of the mouse itself while breathing, would affect image quality. To combat this effect, prospective gating can be employed, where a sensor is placed beneath the mouse and the *in vivo* scanner can time the exposure to match the breath, to minimize image distortion. Cardiac prospective gating is also available, which in similar fashion, times the acquisition of images to the cardiac cycle of the mouse. This is performed by placing ECG electrodes on the two front paws, and a third electrode on one of the hindlegs. (12)

As the use of *in vivo* scanning requires live animals, anesthesia is administered to the animals prior to the scan. Different methods of anesthetic administration are available, such as

intraperitoneal (IP), intramuscular (IM) or inhaled. While the use of IP or IM is more convenient, its administration and titration are often more difficult (placing the rodents well-being at risk), and depending on the research being performed, could negatively affect the project. The main disadvantage with using IP or IM injections, is in the lack of ability to titrate the dose. As the scan times required can be quite lengthy, using inhaled anesthesia provides the benefit of being able to control and adjust the level of anesthesia as needed. With a bolus injection of anesthetic (as is the case with IP or IM), that is not possible, and the researcher runs the risk of not being able to provide adequate amounts of anesthesia for the time required to scan the animal. Additionally, inhaled anesthesia has the benefit of being fast acting, and easily terminated. A drawback however, to inhaled anesthesia is the requirement for complex and expensive equipment, including oxygen delivery and methods of recovering the gaseous anesthetic from the room, to prevent unintended exposure to researchers.

### 1.3 Current Pre-Clinical Contrast Agents

While the use of computed tomography has revolutionized both science and medicine, it isn't without its shortcomings when attempting to view soft tissue structures within the body. Soft tissues, organs or blood vessels are often of similar density and as such, cannot be distinguished from one another when viewed through the lens of CT. (13) To overcome this limitation, the use of intravenous contrast agents has been employed to provide a difference in density between the tissues in question, allowing for their visualization. By introducing the contrast agent, and through threshold manipulation of the image, blood vessels and tumours can be segmented and identified. (13) At the moment, two general groups of contrast agents exist and are currently being used. There are the blood-pool agents which, as the name suggests, tend to have higher retention times

in the vascular system, and are restricted to pre-clinical research with animals, while water-soluble contrast agents are currently used in the clinical setting. Water-soluble contrast agents are organically bound iodine molecules, because iodine provides the highest attenuation available of the non-metal elements. (13) As a generalization, iodine presents itself with relatively low toxicity, but these compounded agents have not been without side effects. They have been responsible for adverse reactions such as allergy and nephrotoxicity, partially due to the extra-vascular pooling of these agents.

As water-soluble iodinated contrast agents are rapidly cleared through the renal system of patients, the window of opportunity to take a CT scan is limited and presents difficulties when these same agents are used in small animal imaging for preclinical research. Mice have extremely accelerated metabolisms, and their entire blood volume is processed and filtered through the kidneys in under 5 seconds. (14) With an average blood volume of 1.5-2.0 ml and a glomerular filtration rate of 0.4 ml per second, it has been shown clinically that 4 seconds after injecting a iodine based contrast agent, it falls to undetectable levels. (15–17) Even with a constant rate infusion of contrast agent, the scans required for small animal imaging are often too long to allow for the amount of contrast agent required for the entirety of the scan time. To overcome these challenges, blood-pool contrast agents have been developed that allow for much longer vascular retention times and stable concentrations within the blood. (18) To allow for longer blood residence times, these iodine-based compounds have had their surface, form and size modified to minimize or alter the speed at which they may pass through the vascular endothelium or are subjected to renal clearance. Such modifications include the use of poly-ethylene glycol, or PEG, which depending on the length of the chain, prevents or minimizes the binding of the iodinated contrast agents to plasma proteins. (18) Some of these contrast agents may also be coupled or

compounded to drugs or delivery agents, with potential to allow for targeting of specific tissues or tumours, for example. In large part however, it is the actual size of the molecules that prevents their excretion through the kidneys. Instead, these blood-pool iodinated contrast agents are excreted through the hepatobiliary system. (13) An example of a blood-pool iodinated contrast agent is Fenestra VC, which consists of iodinated triglycerides formulated in a stable, submicron oil-in-water lipid emulsion. Fenestra has been shown to provide excellent blood retention, however, with its relatively low iodine content, it does not provide strong contrast. (13) Binitio Biomedical Inc. has developed another commercially available blood-pool agent under the name of eXIA160XL which consists of a long-acting aqueous colloidal poly-disperse iodinated solution. (13,19) To address some of the issues associated with iodine-based contrast agents, other metallic elements (including gold) have been studied to determine their effectiveness as potential contrast agents.

### 1.3.1 Gold Nanoparticles as Pre-Clinical Contrast Agents

The use of gold nanoparticles as a contrast agent would appear ideal as gold has both a high atomic number and high density, both of which would provide favourable x-ray attenuating properties. (20) Gold provides an absorption K-edge value of 81 keV vs 33 keV for iodine, and considering that most current clinical CT machines employ 90 - 130 kVp values, gold provides better x-ray attenuation properties. (20) Gold nanoparticles are of particular interest in providing contrast for computed tomography for several reasons including the potential for long circulation times, the ability for conjugation of various functional groups and coatings to target specific tissues, and its general stability. In addition, gold provides approximately 2.7 times greater

contrast per unit weight than iodine, and can also be manufactured in different sizes, and shapes, have their surfaces modified, and are generally considered non-toxic. (20,21)

While gold itself is also considered non-toxic, even in relatively high dosages, in terms of gold nanoparticles however, there have been reports of toxicity associated with specific size ranges. For example, a recent paper reported that injecting unconjugated gold nanoparticles intraperitoneally into mice, ranging in size from 3 to 100 nm, produced some curious results. Unconjugated gold nanoparticles of sizes 3, 5, 50, and 100 nm did not elicit harm, yet those ranging from 8 to 37 nm induced severe sickness in the mice. They exhibited fatigue, change in fur colour, loss of appetite and weight loss. The majority of these mice died within 3 weeks of injection and suffered from camel-like backs and crooked spines prior to death. (22) Another study assessed the effects of citrate-capped gold nanoparticles and their effects on *Drosophila melanogaster* after ingestion. At 15 nm in size, it was noted that there was a severe reduction of their life span and fertility, presence of DNA fragmentation, as well as a significant overexpression of the stress proteins. (23)

When it comes to gold nanoparticle contrast agents, some of the more basic gold nanoparticles used were approximately 30 nm in diameter and PEG-coated to allow prolonged circulation times. The nanoparticles at this size were found to have accumulated in the phagocytic cells of the liver and spleen, with the possibility of their use as targeting contrast agents for hepatocellular carcinomas. Other novel compounds include dendrimer entrapped gold nanoparticles, and acetylated, as well as PEGylated, dendritic nanoparticles of 4-15 nm in size. Mouse studies have shown that in intratumoural injection of the dendrimer-entrapped nanoparticles, the gold nanoparticles are initially taken up by the tumour cells themselves, and eventually accumulate in the liver and spleen of the animal. (20)

Nanoprobes Inc. recently released a proprietary gold nanoparticle formulation under the name of AuroVist™, that consists of particles in the 1.9 nm size range, providing excellent attenuation for imaging of the vasculature, kidneys and tumours. As these particles are so small, their excretion is through the kidneys. In addition, lending to their small size, they also appear to accumulate within tumours and as such, speculation exists that may allow for their usage in x-ray cancer radiotherapy. By allowing for the gold to accumulate in a tumour, for example, and subjecting that tumour to radiation therapy, in theory, the tumour could receive a much higher dose of radiation and therefore, cause what is known as dose enhancement. (24) The accumulated gold nanoparticles create backscatter-induced effects, and where the metal-to-tissue interface is located, much higher dosages of radiation are often found. This in turn may allow the tumour to be exposed to higher radiation dosages when the administered dose remains unchanged. Additional modifications have been made to gold nanoparticles, including CD4-antibody conjugated gold nanoparticles to allow for accumulation in the lymph nodes of mice, lisinopril-coated gold nanoparticles to allow for accumulation in the lung tissues, gold nanoparticles coated with 2-deoxy-D-glucose (2-DG) are used as tumor-targeting contrast agents in cell culture in human A-549 cancer cells, and gold nanoparticles conjugated with UM-A9 antibodies can be used to target squamous cell carcinoma *in vitro*. (20) As is clearly evident, gold nanoparticles have a myriad of potential applications when it comes to providing contrast for targeted tissues, especially tumours.

### 1.4 Tumour Physiology and Imaging

Not uncommonly, tumours have similar densities to their surrounding soft tissues; therefore, to be able to view them under micro-CT, the use of a contrast agent is required. Tumours are often highly vascular with a vascular architecture that is dysfunctional and leads to the leakage

of substances from the vascular system, into the surrounding tumour. This is known collectively as the enhanced permeability and retention (EPR) effect. (25) Using this characteristic to our advantage, and the fact that particle sizes of 200-300 nm can readily extravasate into the tumour tissue (whereas normal tissue has a pore cut-off size of approximately 6-7 nm), nanoparticle contrast media can be used to visualize tumours on micro-CT scans. (14,18) While intravascular injections may lead to accumulation of the contrast media into the tumour over time, direct injection of the gold nanoparticles into the tumour itself would expedite the process and help in retention of the small volume of contrast agent needed.

### 1.5 Histology as the "Gold Standard"

Histology is often referred to as the "gold standard" because it forms the basis of disease diagnosis. By being able to recognize and categorize cells and the tissues and organs that they comprise, this allows for definitive diagnosis and understanding of disease processes. It can be defined as the study of the microscopic structures of the tissues using a light microscope. However, the process itself requires that the specimen in question be sectioned into thin observable slices, stained to visualize specific structures within the tissue sample, and mounted to a microscope slide for viewing. Clearly these additional steps require both time and cost to complete. Often, once the sample has been fixed with formaldehyde, the process of staining commences. Staining is commonly done with the combined hematoxylin and eosin method (H & E) which produces staining of the blue and pink variety. Hematoxylin has an affinity for nucleic acids, and in most methods, RNA and DNA are stained blue. Eosin tends to bind to tissue and cellular components with positive charges, so in practice, the presence of blue or bluish staining indicates the presence of nucleic acids or acidic proteins. (26) Lastly, once the sample has been sectioned, stained and

mounted, it is effectively at its terminal endpoint experimentally speaking. The cells are effectively dead and fixed, and once sectioned, the gross morphology no longer remains. This is an important point, as the site of interest may be quite large (say for example, a melanoma tumour) but sectioning requires that a sample size be chosen. This very much restricts the overall gross morphology and effectively focuses the histological study to a very small site. By focusing on such a small area, it effectively makes it very difficult to correlate with another imaging modality like computed tomography. Not only is the image surface area from histology very small relative to what we see in a micro-CT image, but being able to match and then correlate the two images becomes a challenge. The benefit of having a 3-dimensional imaging modality is not only the increased physical size of the image itself but that by its very nature, a 3-dimensional image can be rotated as needed to allow for alignment and correlation with other imaging modalities. Unlike standard 2D sectioning techniques used for histology under light microscopy for example, optical projection tomography (OPT) provides the advantage of 3D image reconstruction of 2D sections. OPT can be thought of as a macroscopic imaging modality while histology would be considered microscopic in nature.

## 1.6 Optical Projection Tomography

Optical projection tomography is often referred to as the optical analogue to x-ray computed tomography with the added benefit of not requiring ionizing radiation. (27) It also allows for reconstruction of the image, similar to what can be achieved with computed tomography. Compared to histology, there is a great advantage to using OPT as it provides 3D imaging capabilities, allowing the researcher to rotate and evaluate the image similarly to what can be done using CT imaging. As mentioned in section 1.5, histology is a slice through an area of

interest, with the overall gross morphology being lost. OPT on the other hand, allows for complete reconstruction of the image, while retaining that lost morphology. Histology can be thought of as providing a very detailed and focussed image of a very small area of interest, while OPT allows for the "bigger picture" to be seen, in addition to the more minute features of the sample.

The actual process of acquiring an image involves the preparation of the sample by using a fixative such as buffered formalin, followed by embedding of the sample into 1% agarose. Once embedded, and the agarose trimmed, the entire sample must be dehydrated in methanol over several days and cleared in a BABB (1-part benzyl alcohol and 2-parts benzyl benzoate) solution. The sample is then mounted to a magnetic mount and the sample itself is rotated around a vertical axis and a full set of projections taken. These projections are then reconstructed using computer software and the result is an image that can be rotated in three dimensions, similar to what is seen with a CT scanned image.

## 1.7 Rationale

While it is possible to use a contrast agent to assist in isolating and identifying tissues in computed tomography scans, these same contrast agents are not visible when attempting to view them under microscopy. Conversely, the same is true in that stains and dyes used in microscopy can not be viewed under computed tomography. Having a substance that could be used for both micro-CT and microscopy, and also be visible under both imaging modalities without additional staining or preparation would be ideal. Our hypothesis was that by using fluorescently-labeled gold nanorods injected into mice, we could provide contrast for *in vivo* micro-CT imaging, and fluorescence for OPT imaging, while co-localizing the gold nanorods in the two imaging modalities.

In this research project, using an agarose phantom, we attempted to demonstrate that it was possible to visualize the fluorescently-labeled gold nanoparticles under both micro-CT and OPT, and correlate the images. With that objective completed, we showed that these same fluorescently-labeled gold nanoparticles could be used to provide satisfactory contrast under micro-CT when both injected systemically into mice and injected directly into induced murine melanoma tumours. In addition, the goal was to view these particles under OPT imaging as well, and to correlate the images between the two modalities used. Using Cy3 fluorescently-labeled gold nanorods, we showed that they could provide adequate attenuation required for micro-CT imaging and fluorescence required for visual recognition when using UV filtered light with the OPT scanner.

# Chapter 2: Experimental Methods

## 2.1 Overview of Research Project

The research project was divided into 2 general sections, looking first at "proof of concept" by using an agarose model with the gold nanoparticles within, followed by systemic and localized injection of the gold nanoparticles into a mouse model. To illustrate that the fluorescently-labeled gold nanoparticles could be viewed with both micro-CT and OPT imaging, the creation of an agarose block, or phantom, commenced, which contained a 2 µl drop of the gold nanoparticle contrast agent. The agarose phantom was assessed using both a specimen micro-CT scan and OPT.

Once we were satisfied that we could visualize the gold nanoparticles using both of the imaging modalities, and correlate the images, we proceeded to small animal imaging. Ethics approval (A14-0125) was obtained prior to commencing with the small animal research. Having confirmed that the gold nanoparticles were visible, we initially injected mice systemically with gold nanoparticles and viewed them pre-contrast and post-contrast using the *in vivo* micro-CT scanner. Following this, we euthanized the mice, removed the heart, liver and kidneys, and at a much higher resolution, scanned these organs using a specimen scanner micro-CT. The organs were then prepared and viewed using the OPT under UV light.

Subsequently, using additional mice, we induced a melanoma tumour into the right hindleg of the mice, and proceeded to directly inject the same gold nanoparticles into the tumours themselves. Using the same protocol, we performed pre- and post-contrast *in vivo* micro-CT scans, and following euthanasia, we dissected the right hindleg with tumour, and performed a specimen micro-CT scan. These hindleg samples were then prepared and viewed using OPT under UV light. The OPT images were compared with the micro-CT scans and attempts at correlation were made.

All of the mouse handling and scanning procedures were completed at the Centre for High-Throughput Phenogenomics at The University of British Columbia.

## 2.2 Nanoparticles

Two different forms of gold nanoparticles were used for the systemic tail vein injections. The fluorescently-labeled gold nanorods (Nanopartz® Inc., Loveland, CO, USA) were of two varying concentrations, one much higher in actual gold concentration per volume than the other. The manufacturer used optical density per ml to measure the concentration of gold nanoparticles in each sample prior to distribution (see Figure 1). This is an actual measure of the amount of gold present in the sample and according to the manufacturer, extremely accurate. (28) Table 2 illustrates the concentrations in each sample.

Figure 1. Comparison of 50 and 250 OD Nanopartz® gold nanorods

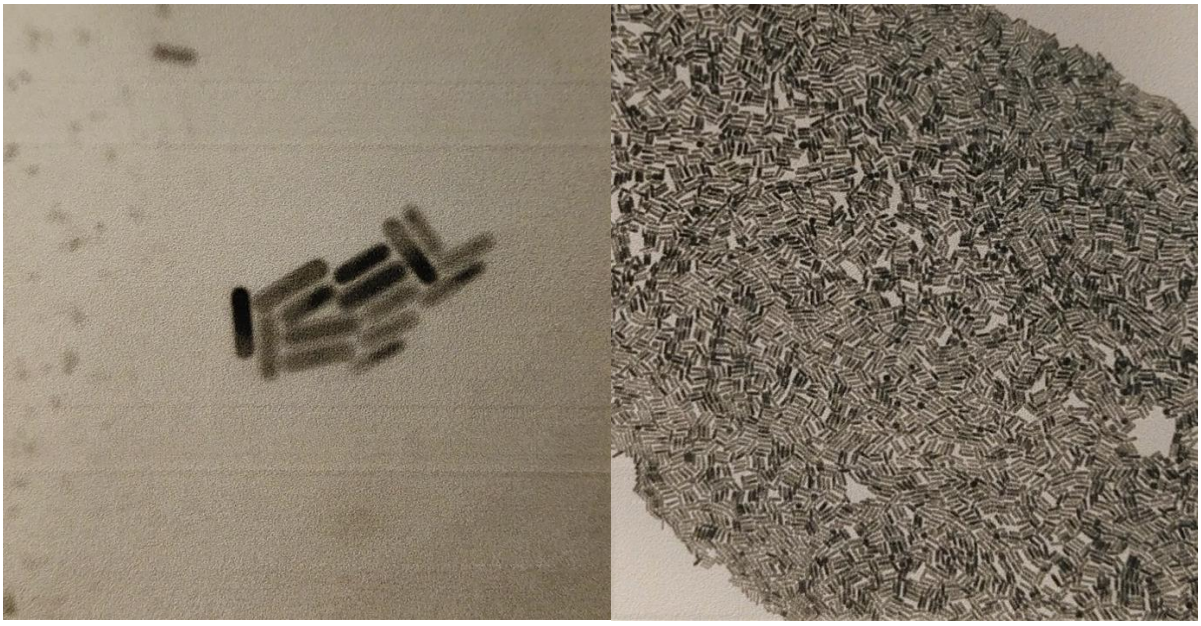

50 OD 250 OD

* Images taken from Certificate of Analysis from Nanopartz® product inserts

These nanorods were 10 x 40 nm in size, coated with Cy3 fluorophore 555/570 nm, and suspended in a sterile PBS solution from the manufacturer. However, as the gold will settle to the bottom of the tube in time, the manufacturer recommended that the tube be agitated for 60 seconds on a vortex mixer, then centrifuged for 60 seconds at 900 RPM. Each time a sample was taken from the tube, the micropipette tip was inserted into the centre of the solution and held approximately in the middle of the remaining solution to ensure reproducible results.

Table 2. Concentrations of Nanopartz® fluorescently-labeled gold nanorods

| | **50 Optical Density** | **250 Optical Density** |
|---|---|---|
| Concentration (nanoparticles per ml) | $5.7 \times 10^{13}$ | $2.1 \times 10^{14}$ |
| Concentration (mg gold per ml) | 3.15 | 12.18 |

The control contrast agent was a naked gold nanoparticle (AuroVist™ 15 nm, Nanoprobes Inc., Yaphank, NY, USA). The purpose to using the AuroVist™ 15 nm, was that literature exists to show that this product will indeed work as a viable micro-CT contrast agent when injected into mice. However, we also wanted to confirm that this product could not be seen under OPT, which is what we expected considering it was not fluorescently-labeled.

## 2.3 Imaging Equipment

### 2.3.1 *In vivo* Micro-Computed Tomography Scanner

All of the *in vivo* scans were done using an *in vivo* micro-CT scanner (eXplore CT 120, TriFoil Imaging,Chatsworth CA, USA) set to 50 microns resolution (Figure 2). When scanning small animals, there are two modes of operation available: gated and anatomical imaging. To address the rapid breathing seen in mice, and resulting image distortion, respiratory gating was

employed, where a sensor (pillow) was placed between the mouse's chest and the scanning bed. Using a physiological monitoring system (BioVet, Spin Systems, (QLD) Pty Ltd, Brisbane, Australia), the resulting change in pressure on the sensor as the mouse breathes allows the *in vivo* scanner to time the exposure to match the breath cycle, thereby minimizing image distortion due to movement. Respiratory gating must be employed to ensure that we obtain motion artifact-free images. (29) The gating was used for the *in vivo* systemic injections only as these mice were being tail vein injected and scanned (these mice had their entire body scanned as these were intravascular injections looking at the circulatory system as a whole).

Anatomical imaging can be employed to assess a specific site of a mouse's anatomy. In our case, because the tumour was grown in the right hindleg and injected directly, therefore a full

Figure 2. TriFoil eXplore CT 120 *in vivo* micro-CT scanner

body scan was not necessary. The site in question was free of movement and did not require gated imaging.

Table 3 below outlines the imaging protocols employed for the *in vivo* micro-CT imaging of both the systemic injections and direct tumour injections:

Table 3. Imaging protocols for *in vivo* micro-CT

| Scan Type | Respiratory-Gated | Anatomical Soft Tissue | Anatomical Bone |
|---|---|---|---|
| Protocol Name | Systemic Injection Step and Shoot | Tumour Injection Step and Shoot | Bone Low Noise |
| Voltage (kVp) | 80 | 80 | 100 |
| Current (mA) | 40 | 40 | 50 |
| Exposure Time (ms) | 100 | 100 | 20 |
| Bin Mode | 1 x 1 | 1x1 | 2x2 |
| Resolution (μm) | 25 | 25 | 50 |
| Number of Views | 220 | 220 | 720 |
| Scan Time (min) | 10-20 (depends on rate) | 8.5 | 22.5 |
| Scout Dose (Gy) | $555\times10^{-6}$ | $563\times10^{-6}$ | $584\times10^{-6}$ |
| Entrance Dose (Gy) | $303.6\times10^{-3}$ per phase | $315.9\times10^{-3}$ | $840\times10^{-3}$ |

### 2.3.2 Specimen Micro-CT Scanner

A specimen micro-CT machine (Scanco Medical μCT100, SCANCO Medical AG, Brüttisellen, Switzerland) was used for all high-resolution scans (Figure 3). Depending on the size of the sample, 10 to 17.2 micron resolution was used. In the tumour injection portion of the research project, mice #1, 2 and 3 had tumours that were excessively large and those three samples were scanned at 17.2 microns to keep scan times and the resulting data set smaller, while the remaining mice were scanned at 10 microns.

Figure 3. Scanco Medical µCT100 specimen scanner


The imaging protocols for the specimen scanner for mouse #4-15 included energy at 90 kVp, and an intensity of 200 µA. For mouse #4-6, the voxel size was 17.2 microns, at a scan time of 87 minutes. For the remaining mice, #7-15, voxel sizes were all 10 microns, with scan times ranging from 109 – 144 minutes.

### 2.3.3 Optical Projection Tomography

The Bioptonics OPT Scanner 3001M (MRC Technology, Edinburgh, Scotland, UK) was used for all optical projection tomography imaging (Figure 4).

Figure 4. Bioptonics OPT scanner 3001M

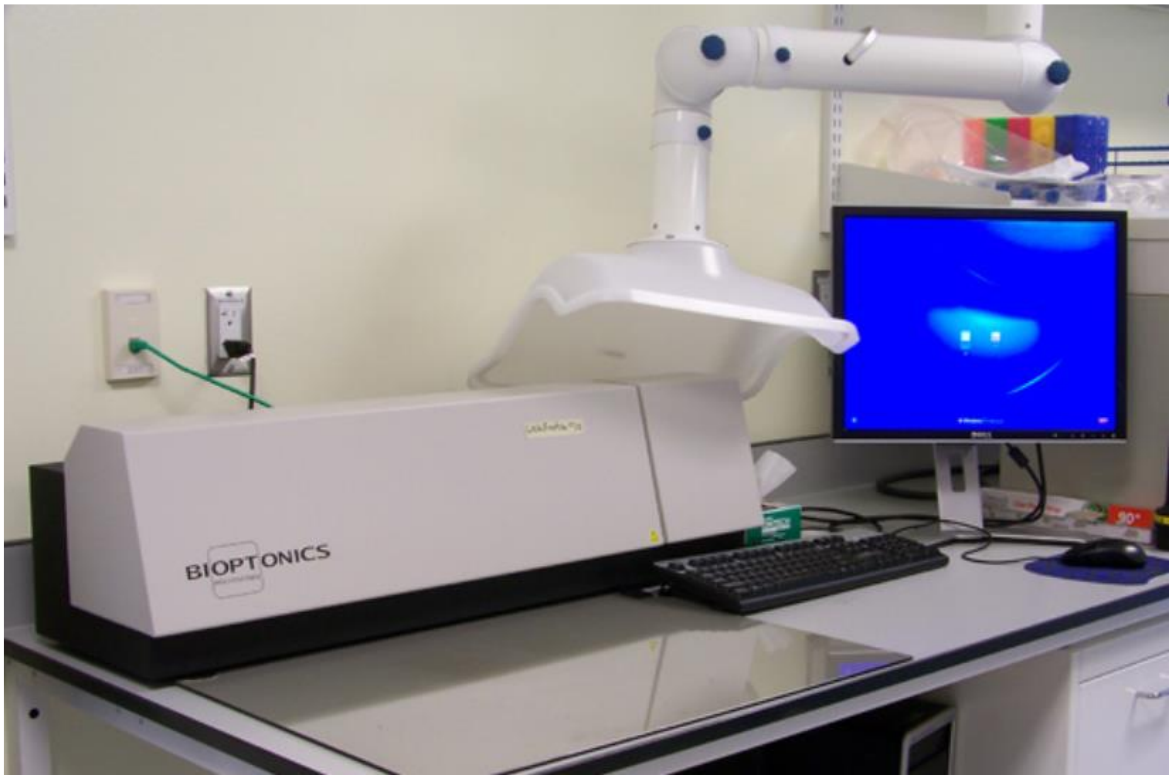


To view the sample under OPT, it must be embedded first into agarose, and allowed to set. Once trimmed, it must go through a process known as clearing to provide a sample as transparent as possible. This cleared sample is then adhered to a mount and scanned while submerged in BABB within the cuvette. The imaging protocols for the agarose phantom included an image pixel size of 10 µm and an exposure of 1000 ms. For mouse #1-3, we used an image pixel size range of 12 – 20 µm and an exposure range of 150-200 ms (settings were used for the excised organs). Lastly, for mouse #7-15, we used an image pixel size of 20 µm and an exposure range of 300 - 600 ms (settings were used for right hindleg and tumour). The light source used was filtered UV light at 545-610nm wavelength, to correspond with the Cy3 fluorophore on the gold nanoparticles.

## 2.4 Agarose Phantom Experiments

A solution of 1% agarose was prepared using 0.25 g of agarose powder, dissolved in 25 ml of laboratory distilled and filtered water, heated through on a heating element. Once dissolved, the solution was poured into a disposable hexagonal polystyrene weighing dish and allowed to cool. Once having reached the point of having thickened but still remaining relatively fluid, using a micropipette, we deposited 2 µl of the 50 OD Nanopartz® gold nanorods into the centre of the agarose solution and allowed it to set in the refrigerator at 4 degrees Celsius. Care was taken to try and ensure that the product stayed in a tight grouping and did not dissipate throughout the gel, hence the timing of the agarose setting was important. If the agarose was too fluid, the nanoparticles would begin to bleed and dissipate throughout the agarose. However, if the agarose was too firm, the introduction of the micropipette would cause the agarose to tear and result in the introduction of air bubbles. By placing the agarose to cool on a bed of ice, approximately 15 minutes wait time was needed to achieve the proper consistency. Once the agarose had fully set with the nanoparticles encased within it, it was trimmed to approximately 1 $cm^3$ using a standard shaving razor, and the phantom extracted from the weighing dish.

The phantom was scanned first using the specimen micro-CT scanner. The phantom was wrapped loosely in a water-moistened paper towel and placed into a 15 ml Falcon® tube. This tube was inserted into a 19 mm specimen micro-CT holder. Following the specimen scan, the agarose phantom was cleared by soaking the agarose phantom in 100% methanol (30 ml) for a total soak time of 43 hours. The methanol was replaced with fresh methanol, at time points of 2, 6, and 19 hours, after which, it was placed into BABB (1-part benzyl alcohol and 2-parts benzyl benzoate) for an additional 24 hours. The agarose phantom was then removed from the BABB, blotted dry on a paper towel and using super glue (Instant Adhesive 200, Permabond LLC,

Pottstown, PA, USA), it was adhered to the mount (see Figure 5). Using the parameters outlined previously, the OPT scan was completed.

Figure 5. Sample in agarose block (arrow) adhered to mount, positioned above cuvette

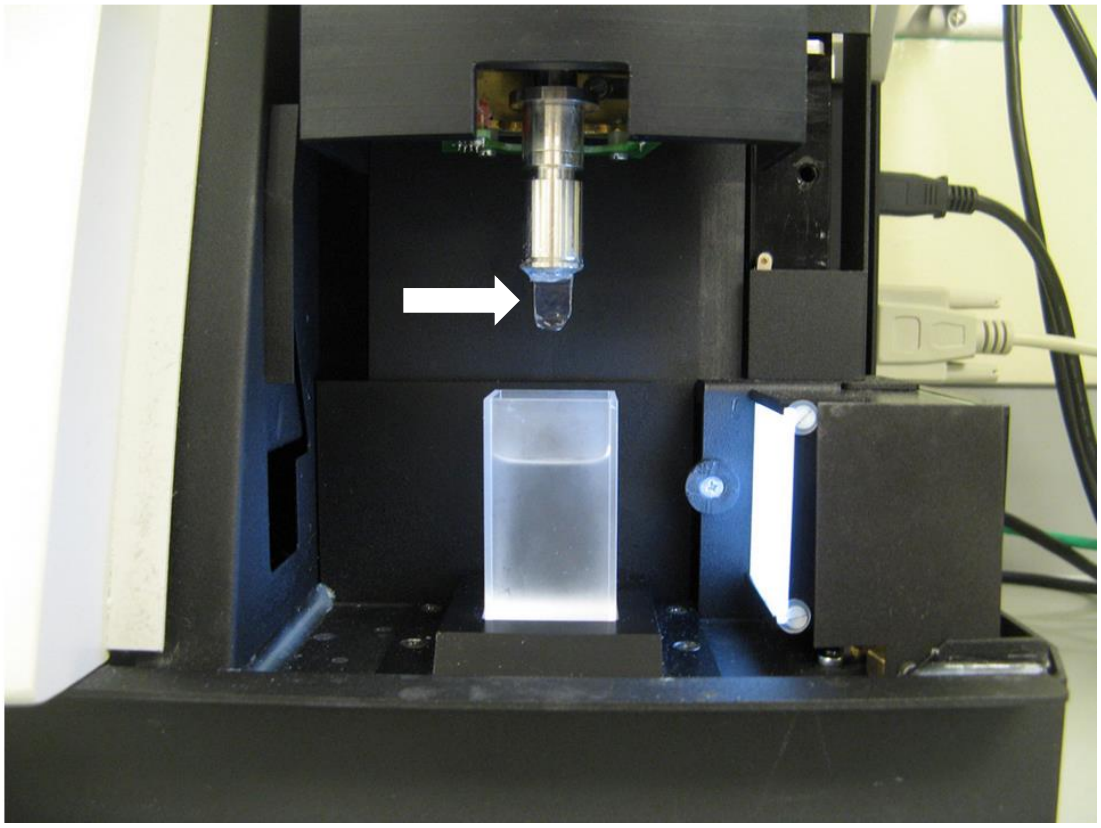

## 2.5 *In Vivo* Experiments

### 2.5.1 Systemic Injections

Ethics approval (A14-0125) was obtained prior to commencing with the small animal research. Three, female nine-week-old CD-1 mice were purchased from Charles River (Wilmington, MA, USA) and housed in an enclosure at the Modified Barrier Facility at The University of British Columbia. The mice were fed a standard mouse diet with free access to food

and water and allowed to acclimate for a period of 3 days prior to commencement of research. During their stay with animal care, they were subjected to a standard day and night cycle.

All scans and injections were performed on anesthetized mice, using an inhaled anesthesia machine providing 5% isoflurane in $O_2$ in the induction chamber and once transferred to the scanning bed, 1.5 - 2% isoflurane in $O_2$ as maintenance using a nose cone, during the scans (Figure 6).

Figure 6. Mouse under inhaled anesthesia on micro-CT scanner bed

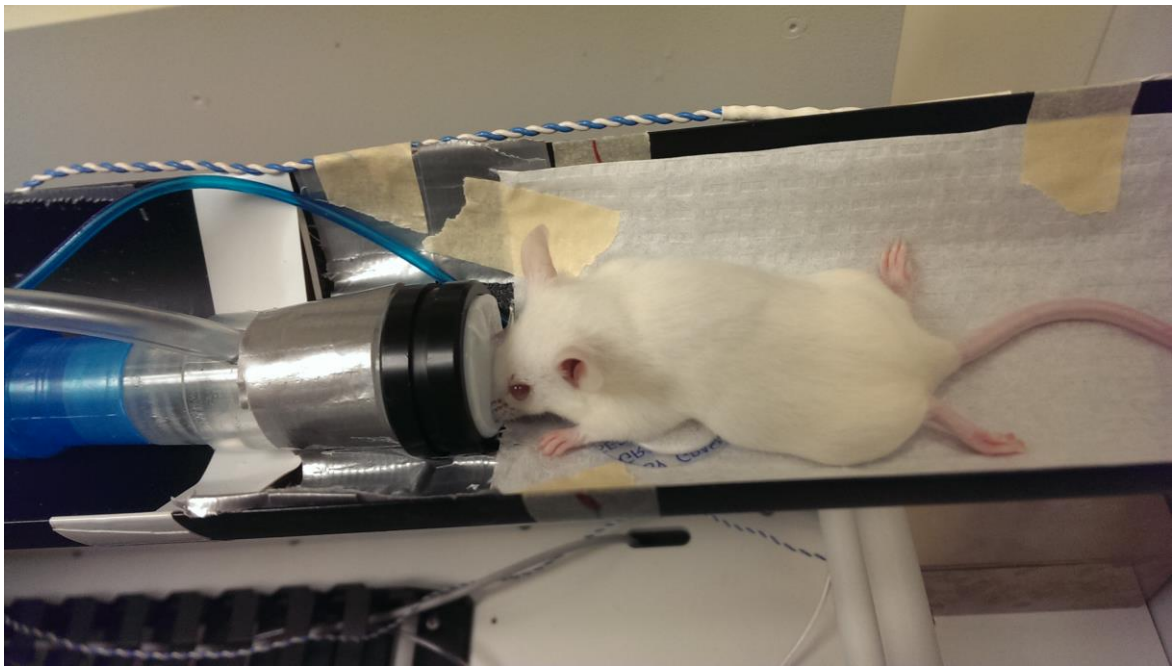

At all times, while anesthetized, the mice were kept warm with gel heating pads to approximately 37 degrees Celsius. In addition, eye lubricant gel was placed on the eyes of the mice during any and all procedures while under anesthesia.

Figure 7. Anesthetized mouse ready for tail vein injection (tail vein is visible)

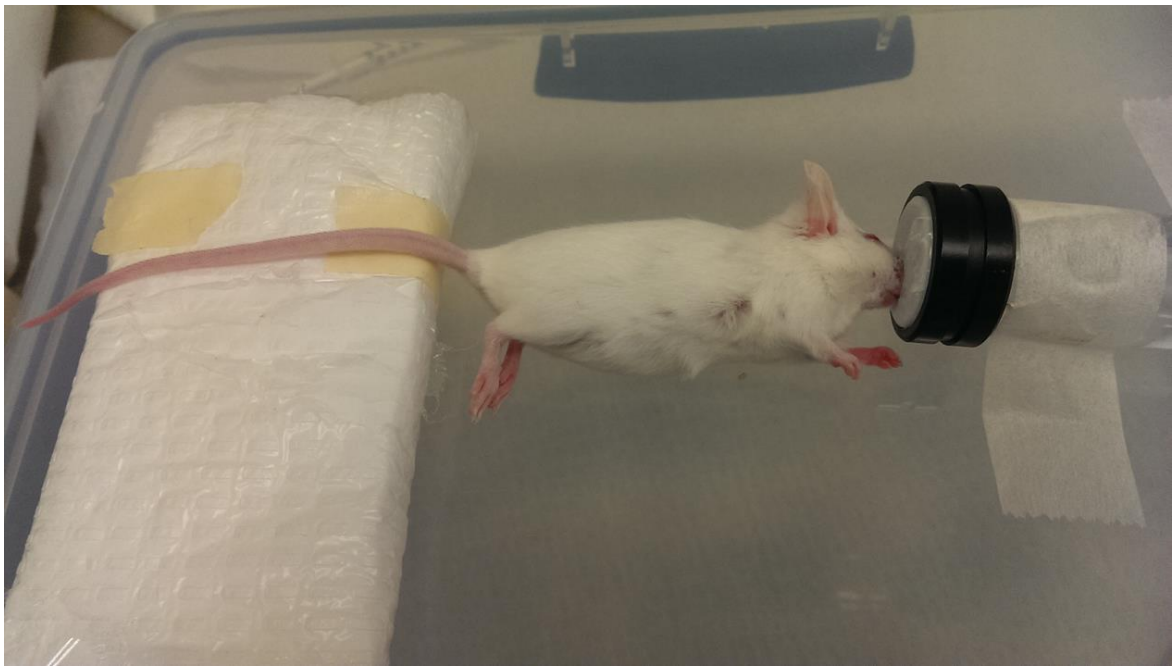

The initial pre-contrast scans were completed by transferring the mice from the induction chamber, immediately to the scanning bed where the nose cone with anesthetic was waiting. After applying heating pads, the mice were introduced into the *in vivo* micro-CT scanner and a scout view was taken to ensure that the region of interest was positioned properly, prior to their pre-contrast scans using respiratory gating. The mice were laid prone onto the scanning bed, where a pressure sensitive, respiratory monitoring sensor (pillow) was placed beneath the diaphragm. This pressure transducer transmits the movement of the diaphragm (breathing) to a recording of a respiratory wave signal, corresponding to end expiration. (12,30)

After the pre-contrast scan was complete, the mice were gently removed from the scanning bed and placed on a prepared area, staged for the tail vein injection. As the systemic tail vein injections were performed off the scanning bed and using a foam block to prop the mouse tail for the tail vein injection (see Figure 7), the nose cone was also used to maintain anesthesia. Once the

mice were positioned on their left side, with their tail resting on the tail prop (Figure 7) and kept warm with a heating pad, the mouse tail was wiped with an alcohol wipe to disinfect the injection site. Using a 1 ml insulin needle of 29-gauge, 200 µl of the contrast agent was introduced into the lateral tail vein (near the base of the tail where the vein was most prominent).

For the *in vivo* systemic injection portion of the project, three mice were injected with either 200 µl of 50 OD Nanopartz® gold nanorods (Mouse #1), 200 µl of AuroVist™ 15nm (Mouse #2), or 200 µl of 250 OD Nanopartz® gold nanorods (Mouse #3). The specifics of each mouse can be found in Table 4 below:

Table 4. *In Vivo* Systemic Injection Parameters

| **Mouse #** | **Weight (g)** | **Contrast Used** |
|---|---|---|
| 1 | 29.3 | 50 OD Nanopartz® |
| 2 | 32.7 | AuroVist™ 15 nm |
| 3 | 28.1 | 250 OD Nanopartz® |

Once injected, hemostasis was achieved using gentle pressure with a piece of gauze, and the mice were quickly placed onto the scanning bed, in a prone position, with the respiration sensor beneath their diaphragm for a respiratory gating scan. Heating pads remained in place throughout the scans, using the *in vivo* micro-CT scanner for both a pre and post-contrast scan. The resolution of the scans were 50 microns.

Once the post-contrast scan was complete, the mice were then euthanized with a lethal IP injection dose of Avertin (500 mg/kg) using a 3 ml syringe and 25 gauge, 1" needle. The Avertin was prepared by dissolving 2.5 grams of Tribromoethanol in 5 ml amylene hydrate and heating it to 40° Celsius, while stirring. Distilled water was added slowly, while continuing to stir, up to a final volume of 200 ml. This solution was then placed into a glass vial, wrapped in tin foil to protect it from the light. As prepared, this solution contained 12.5 mg of Tribromoethanol per ml

and once refrigerated, had an expiration date of 2 weeks. As soon as the Avertin injection was given through IP, the mouse was returned to the induction chamber, and 5% inhaled isoflurane was administered until the mouse had expired.

Once euthanized, a post-mortem scan was taken with the *in vivo* micro-CT scanner (see Table 3, Anatomical Bone Scan protocol), after which the heart, kidneys and liver were dissected and placed into 10% buffered formalin to be fixed. Attempts were made to tie off the blood vessels to the organs as they were dissected, to retain as much blood within them as possible. After a period of 3 days in formalin, the organs were removed, wrapped with a minimal amount of moist paper towel to stabilize them and placed into a 15 mL polystyrene conical tube (Falcon®, Corning Science Mexico S.A. de C.V., Reynosa, Tamaulipas, Mexico). The samples being scanned were wrapped loosely in a piece of water moistened, paper towel to prevent movement during the scanning procedure. The paper towel provided additional thickness and body to the sample, ensuring it would remain in place in the tube during the rotations in the specimen scanner. The Falcon® tubes were placed into the appropriate specimen micro-CT holder (19 mm in size) and loaded into the specimen scanner. Prior to the scanning procedure, a scout view was taken to ensure that the region of interest was positioned properly. The organs were scanned using the specimen micro-CT scanner (at 7.5 microns for the heart and kidneys and 10 microns for the liver).

Once complete, they were placed into a prepared and slightly cooled, 1% agarose solution in a hexagonal weighing dish, allowed to set completely in the refrigerator, and the agarose trimmed. In preparation for the OPT, the samples were all soaked in 100% methanol (30 ml) for a total soak time of 43 hours. The methanol was replaced with fresh methanol, at time points of 2, 6, and 19 hours, after which, it was placed into BABB (1-part benzyl alcohol and 2-parts benzyl benzoate) for an additional 24 hours. These samples were kept out of direct light and the caps on

these bottles were loose to allow for escape of the residual methanol. Once cleared, all of the samples were placed in paper towels to remove excess BABB and adhered to the OPT mount using super glue. The samples were scanned at 150 ms exposure time for Mouse #1 and 2, and 200 ms for Mouse #3. Once completed, these samples were stored in BABB, away from direct light.

### 2.5.2 Murine Melanoma Cell Culturing

B16-F10 cells were purchased from ATCC® (CRL-6475™, American Type Culture Collection, Manassas, VA, USA) and were grown in uncoated cell culture-grade dishes in Dulbecco's modified Eagle's medium (DMEM, Cat#: ATCC-302002) containing 10% fetal bovine serum and penicillin-streptomycin (Fetal Bovine Serum, Cat#: 12484-010, Gibco™, Merck KGaA, Darmstadt, Germany).

Prior to injection, the culture medium was removed, and the cell layer was rinsed with phosphate-buffered saline (PBS, Cat#: 20012-027, Gibco™, Merck KGaA, Darmstadt, Germany) to remove all traces of serum that contained trypsin inhibitor. We then added 1.0 mL 0.25% (w/v) Trypsin -EDTA solution (Cat#: 25200-056, Gibco™, Merck KGaA, Darmstadt, Germany) and observed the cells under an inverted microscope until the cell layer was dispersed and the cells detached. Next, we added 4.0 mL of complete growth medium, aspirated the cells with gentle pipetting into a 15 mL Falcon tube. Cells were washed with PBS and cell numbers were counted using a hemocytometer. After spinning at approximately 125x G for 5 minutes, B16-F10 cells were re-suspended in PBS at a concentration of $3x10^5$ cells per ml.

### 2.5.3 *In Vivo* Tumour Injections

Twelve, female nine-week-old C57Bl6 mice were purchased from Charles River (Wilmington, MA, USA) and housed in an enclosure at the Modified Barrier Facility at The University of British Columbia. The mice were fed a standard mouse diet with free access to food and water and allowed to acclimate for a period of 3 days prior to commencement of research. During their stay with animal care, they were subjected to a standard, day and night cycle. All scans involving live mice included inhaled anesthesia (5% isoflurane induction dose with 2% maintenance dose, with oxygen). In addition, eye lubricant was applied to the eyes of all mice under anesthesia.

Mouse #4-6:

Under inhaled anesthesia, the mice were subcutaneously injected with 0.1 ml of the murine melanoma cell solution in the right hind leg, approximately in the mid-point of the femur, with the mouse lying in the prone position. The mice were returned to the animal facility for 3 weeks, with daily monitoring by the staff to ensure the mice weren't showing signs of stress or pain. The expected tumour size was $1cm^3$; however, the first three mice did in fact have tumours that were much larger than the remaining mice used. All mice had their tumours measured using calipers but as these were invasive tumours, it wasn't always easy to determine where the border of the tumour was, relative to the epidermis and fur on the mouse. In addition, some of these tumours appeared to grow at exponential rates, changing dramatically in size over a night or two. These first 3 mice, which had very large tumours, were allowed to have their tumours grow for a period of 3 weeks. When we realized that these tumours were in fact too large, we revised the protocol

for the remaining mice, to focus on tumour size, taking care that they did not grow beyond the target size of 1 $cm^3$.

Once the 3 weeks of tumour growth had passed, the 3 mice were transported to the micro-CT room from the animal care facility. Under inhaled anesthesia, after induction in the chamber with 5% isoflurane and $O_2$, the mice were transported gently to the scanner bed where a nose cone was placed to maintain anesthesia using 1.5 – 2% isoflurane and $O_2$. The mice were kept warm with a heating pad and once the pre-contrast scan was completed (see Table 3, Anatomical Soft Tissue Scan protocol), care was taken to not move the mouse for the contrast injection (which would allow for more accurate registration). The mouse remained on the scanning table under anesthesia and was not recovered between scans. The tumours were directly injected with 20 µl of 250 OD Nanopartz® gold nanorods using a 1 ml insulin needle of 29 gauge. When the injection of gold nanorods was completed, the needle was left in place for 10 seconds, to ensure the contrast had time to enter the tumour. A post-contrast scan was immediately performed at a resolution of 50 microns. The mice were never recovered from the inhaled anesthesia and once the final post-contrast scan was complete, the mouse was transported back into the induction chamber, maintained for another minute or so under 1.5 – 2% isoflurane and $O_2$, and were then euthanized with inhaled 100% carbon dioxide ($CO_2$). Once, euthanized, the fur of the right hind leg, where the tumour was present, was removed with a commercially available hair removal product (Nair®). The hind leg was subsequently dissected with a #10 scalpel, taking care to ensure the entire tumour was removed. The dissected right hind leg was placed in 40 ml of 10% buffered formalin for 2 days, after which it was scanned with the specimen micro-CT scanner.

The right hindleg samples were removed from the formalin, padded dry and loosely wrapped in a paper towel. They were then inserted into a 50 ml sized Falcon® tube, placed into a

34 mm specimen holder, and scanned with the specimen micro-CT scanner at a resolution of 17.2 microns. Once the scan was complete, the samples were placed back into the formalin solution. Unfortunately, the hindleg and tumour were too large to be scanned with the OPT scanner, and were therefore not prepared for OPT. There is a functional size limit to the size of sample that can be scanned. If the sample is too large to be mounted and rotated in the cuvette, it can not be scanned.

Mouse #7-15:

With respect to mouse #7-15, these mice had tumours that did not exceed the 10 $mm^3$ threshold and as such were able to be subjected to OPT scanning. In the exact same manner as described for mouse #4-6, the same protocols were followed for the *in vivo* scanning and specimen micro-CT scans. As these samples were smaller, 15 ml Falcon® tubes were used, with the 19 mm specimen holders. As a result, the resolution used for the specimen micro-CT scanner was 10 microns.

Once the specimen scan was complete, we were concerned that due to the size of the samples, that the penetration of clearing would be inadequate, so it was decided to first clear the right hindlegs alone, then embed them in agarose and clear them once more with the agarose. The right hindlegs were placed in 40 ml of 100% methanol, which was replaced daily for 4 days, after which it was placed in 40 ml of BABB for 2 days. These samples were kept out of direct light and the caps on these bottles were loose to allow for escape of the residual methanol. Once cleared, the samples were then placed into 1% agarose, which was allowed to cool and set in the refrigerator, after which it was trimmed to ensure it would fit in the OPT cuvette. The agarose embedded right hind leg was placed once again into 40 ml of 100% methanol for 4 days (the

methanol was replaced daily) after which it was placed into 40 ml of BABB for 2 days. This was done to clear the agarose surrounding the sample. The samples were then scanned with the OPT scanner at exposure times of 300-600 ms using filtered UV light at 545-610nm wavelength. Upon completion, the entire sample in agarose was placed back into the BABB solution and stored away from direct light.

## 2.6 Data Analysis

MicroView (Version ABA 2.2, Trifoil Imaging, Chatsworth USA), on a Linux based PC was used to view the pre- and post-contrast *in vivo* micro-CT scans. The pre and post-contrast *in vivo* scans were registered using 6 reference points from the right hindleg of each mouse in the tumour injection study. By using the same reference points on both the pre- and post-contrast images, it was possible to register the two images and allow for scrolling between the two in the same planes. A rigid-body registration algorithm was used. We also assessed and viewed the specimen micro-CT scans and OPT scans, using MicroView, with additional viewing of the scans being done with Amira (Version 6.0.1, Thermo Fisher Scientific, Waltham, Massachusetts, USA) on a Windows based PC.

### 2.6.1 Tumour Measurements

The tumours on mouse #4-15 were measured not only clinically with digital calipers, while the mice were being housed and monitored in the animal facility, but they were also measured using the MicroView software (see Table 5 and 6). The *in vivo* scans were assessed using MicroView using the built-in Region of Interest feature. The software allows the user to browse through the slices of the micro-CT scan and to manually outline the margins of the region of

interest (in our case, the perceived melanoma tumour). The clinically measured tumour size was approximated using the calipers but as the tumours were invasive and penetrated the soft tissue, a 3rd measurement to determine depth was not possible. However, using the formula of $V = (W^2 \times L)/2$, where V represents volume, W represents width and L represents length, we can effectively estimate the volume of the tumours. (31)

# Chapter 3: Results

## 3.1 Agarose Phantom

The results of the phantom testing using 2 µl of 50 OD Nanopartz® gold nanorods in 1% agarose were promising and provided proof of concept. Figure 8 is a 3D volume rendered image that illustrates the ability of the gold nanoparticles to fluoresce when subjected to UV light in the 545-610 nm wavelength range using OPT (left). The image also shows that the gold nanoparticles were visible under high resolution micro-CT specimen scanning (right). The grouping of the white spots was indicative of our attempt to keep the drop of contrast agent as contained as possible within the agarose gel, as it was setting. When scanned using micro-CT and OPT and the two images compared, the phantom images could be correlated.

Figure 8. Co-localization between OPT (left) and high-resolution micro-CT (right)

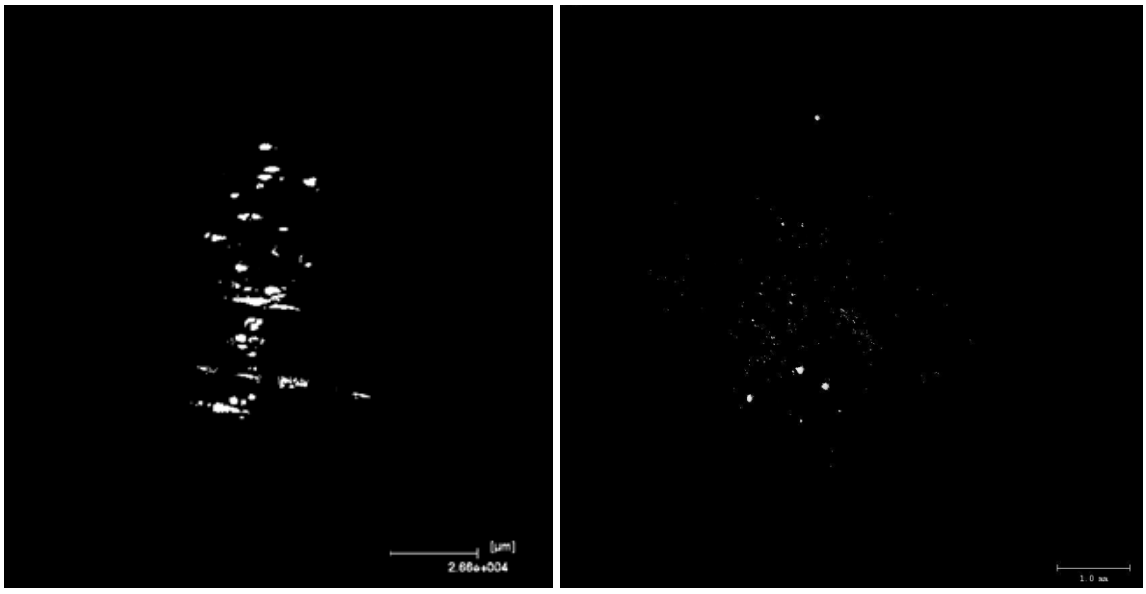

## 3.2 *In Vivo* Systemic Injections

Mouse #1 was tail vein injected with the 50 OD Nanopartz® gold nanorods but the results revealed that the fluorescently-labeled gold nanoparticles could not be visualized in the micro-CT nor in the OPT scans (see Figure 9). There was some doubt as to whether the injection had actually entered the tail vein, and whether the 50 OD concentration was enough to provide contrast.

Figure 9. OPT images of Mouse #1 after tail vein injection of 200 µl of 50 OD Nanopartz® gold nanorods (from left: heart, kidney and liver)

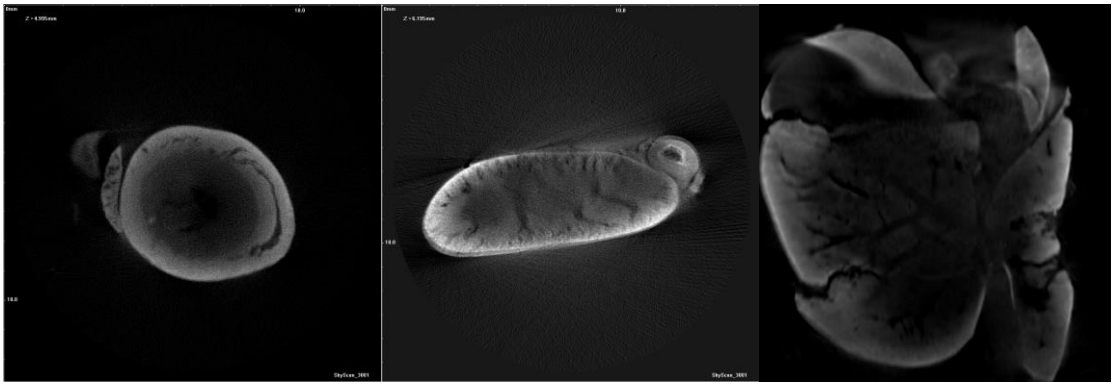

Mouse #2 was tail vein injected with the AuroVist™ 15 nm and after scanning the mouse post-contrast with the micro-CT scanner at 50 microns, there was no contrast evident. As these nanoparticles were not fluorescently-labeled (they were naked gold nanoparticles) the mouse organs were not extracted and scanned with the OPT.

Mouse #3 was tail vein injected with the higher concentration of the 250 OD Nanopartz® fluorescently-labeled gold nanorods, and as with the 50 OD nanorods, the contrast was not visible on the micro-CT scans. Figure 10 and 11 illustrate that the contrast was not visible. These nanorods were fluorescently-labeled so after the mouse was euthanized, the heart, kidneys and liver were excised and subjected to OPT scanning. Unfortunately, the results mirrored the 50 OD

nanorods, in that no contrast could be identified in the OPT scans, as shown in Figure 12. It is possible that the tail vein injection was missed and therefore, the contrast never introduced into the bloodstream. Even if the tail vein injection was successful, once the contrast entered the bloodstream, it may have been diluted to such a level that it would no longer be visible on micro-CT or OPT.

Figure 10. Images of micro-CT scan of Mouse #3 at 50 microns after tail vein injection of 200 µl of 250 OD Nanopartz® gold nanorods

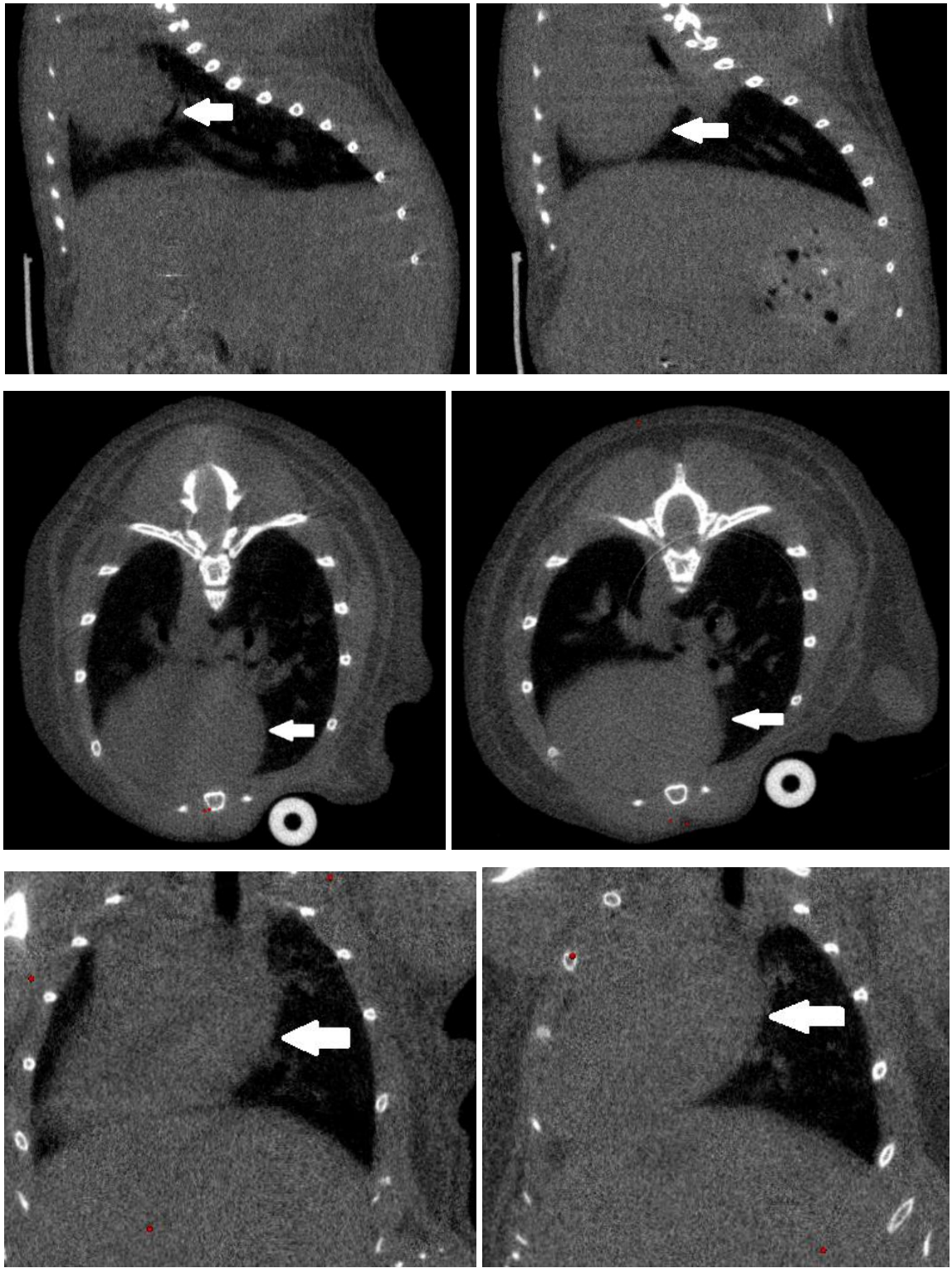

Left image is pre-contrast and right image is post-contrast (arrows point to heart)

Figure 11 Images of micro-CT scan of Mouse #3 at 50 microns after tail vein injection of 200 µl of 250 OD Nanopartz® gold nanorods. The dots around the midsection are indicative of metal particles found in mouse feed.

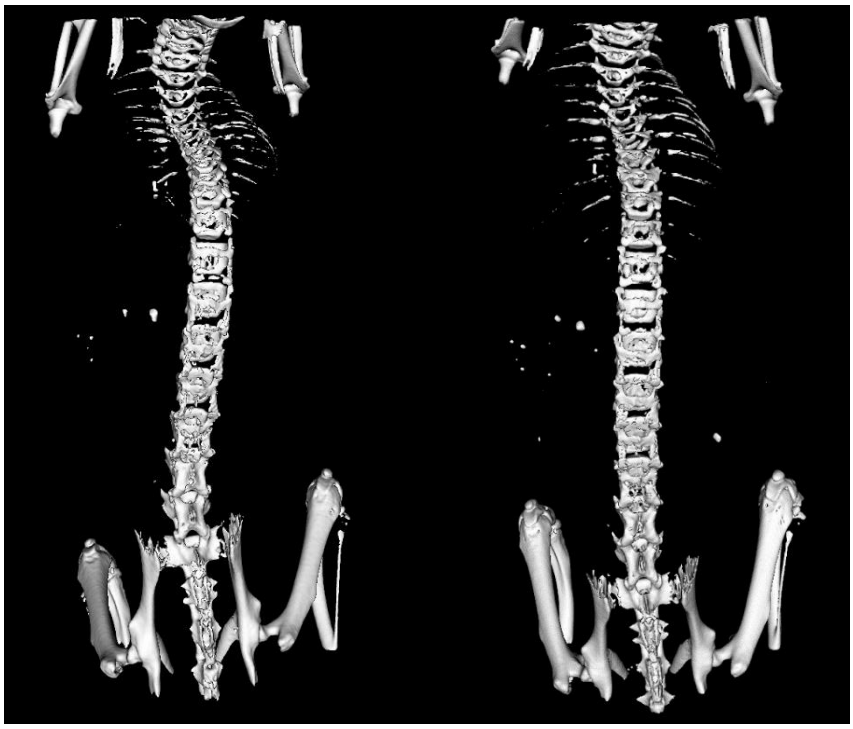

Left image is pre-contrast and right image is post-contrast

Figure 12. OPT images of Mouse #3 after tail vein injection of 200 µl of 250 OD Nanopartz® gold nanorods (from left: heart, kidney and liver)

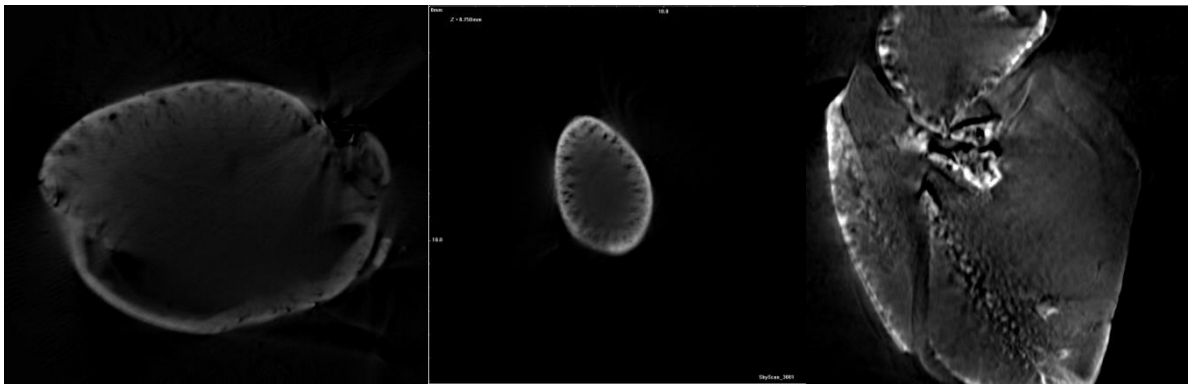

### 3.3 *In Vivo* Tumour Injections

We selected 3 mice to present, all representing varying degrees of contrast visualization. Mouse #10 provided the most successful visualization of the melanoma tumour using the fluorescently labeled gold nanorods, in both micro-CT and OPT. The tumour could be easily visualized, in both the *in vivo* and specimen micro-CT scan, and interestingly the OPT also provided us with a fluorescent signal not only from the contrast agent, but also from the surrounding muscle tissues. In fact, the muscle striations could be visualized as well.

Mouse #12 provided what was considered moderate contrast, and while the contrast agent was visible under both *in vivo* and specimen micro-CT, it wasn't well enough distributed to provide adequate tumour contrast. The OPT also provided us with a fluorescent signal, however, as with the micro-CT images, a well-defined tumour could not be seen. Lastly, mouse #8, provided us with what was deemed the least successful signal. Not only was the contrast not visible on the *in vivo* images, but it also wasn't seen on the much higher resolution scan of the specimen micro-CT. And as expected, the OPT did not appear to show the contrast signal (or rather, the soft tissue signal washed out any possible contrast agent fluorescence).

It should be noted that we were unable to visualize and assess the tumour found in mouse #14, both pre and post-contrast administration. From the *in vivo* micro-CT scans, it was noted that the contrast agent was not in fact present in the tumour itself but appeared to have leaked out of the injection site and deposited itself in the fur of the mouse. This was verified because on the *in vivo* scans, the contrast can be seen on the outer most surface (fur) of the right hind leg, while when viewing the specimen scan (which was taken after the fur was removed), the contrast was no longer visible.

While the mice were monitored daily, and their tumour size assessed using calipers, the actual tumour sizes themselves varied considerably between the mice at the point of euthanasia. In particular, mouse #4-6 had tumours that were much larger than the remaining mice, which was due to the fact that these mice were allowed to grow their tumours for 3 weeks. The remaining mice were monitored until the sizes of the tumours dictated their experimental end points. Using MicroView software with the built-in region of interest function, and using the *in vivo* post-contrast micro-CT scans, we were able to estimate the borders of each tumour and have the computer software calculate the corresponding size of the tumour volume (Figure 13). These calculations were done with the *in vivo* micro-CT scans obtained after the tumours had been injected with 20 µl of the gold nanorod solution (12.18 mg/ml). By viewing cross-sections of the micro-CT scans, and manually outlining the perceived tumour borders in these sections (as shown in the left-hand images in Figure 13), the computer is able to generate a 3D image of the measured tumour, or region of interest (right-hand images in Figure 13). Table 5 and 6 shows the variability in assessed tumour volumes using the region of interest function, in addition to the actual clinically measured tumour dimensions and their estimated volumes. There was clearly some variability between the mice themselves but also between what we measured using software and estimated clinically. Some of the tumours that were measured as being quite large using the software, were estimated to be much smaller using the calculated volumes from our caliper measurements.

Visualization of the gold nanoparticles in the *in vivo* images was possible although the results varied from very little or no contrast being evident in some scans, to being able to differentiate the tumour very well from the surrounding tissues in other scans. By employing the registration feature present in MicroView, we used 6 points present on hard tissue (in this case, bone within the region of the right hind leg where the tumour was isolated, was used) to effectively

register the pre- and post-contrast administration images and allow for comparison. Mouse #10 for example, produced a very detailed tumour outline with contrast clearly present, allowing for excellent visualization of the tumour.

Having gone through the slices, the software reconstructed the slices into a 3D region of interest (Figure 13) and provided a volume measurement of the area (column 3 of Table 5 and 6). Figure 14 shows three mice that provided very good contrast results (mouse #10), adequate contrast (mouse #12) and poor contrast (mouse #8).

Table 5. Mouse tumour features at pre-contrast injection (tumours > 1cm$^3$ as image-based tumour volume)

| **Mouse** | **Weight (g)** | **Image-Based Tumour Volume (mm$^3$)** | **Clinically Measured Tumour Dimensions (mm)** | **Estimated Tumour Volume (mm$^3$)** |
|---|---|---|---|---|
| 4 | 25.6 | 7575.6 | 13x13 | 1099 |
| 5 | 23.2 | 2910.7 | 12x12 | 864 |
| 6 | 23.8 | 2555.5 | 11x11 | 665 |
| 11 | 21.8 | 1099.0 | 10x10 | 500 |

Table 6. Mouse tumour features at pre-contrast injection (tumours ≤ 1cm$^3$ as image-based tumour volume)

| **Mouse** | **Weight (g)** | **Image-Based Tumour Volume (mm$^3$)** | **Clinically Measured Tumour Dimensions (mm)** | **Estimated Tumour Volume (mm$^3$)** |
|---|---|---|---|---|
| 7 | 19.0 | 605.0 | 10x10 | 500 |
| 8 | 18.7 | 859.0 | 10x10 | 500 |
| 9 | 19.1 | 506.8 | 9x9 | 365 |
| 10 | 18.2 | 436.4 | 9x9 | 365 |
| 12 | 20.6 | 404.4 | 8x8 | 171 |
| 13 | 20.4 | 837.9 | 9x9 | 365 |
| 14 | 20.6 | Could not assess | 8x8 | 171 |
| 15 | 21.3 | 219.0 | 8x8 | 171 |

Figure 13. Images showing the Region of Interest function, outlining the visualized tumour post-contrast injection, for *in vivo* micro-CT scan at 50 microns resolution. Left image is single slice through tumour with margins outlined, and right image is 3D region of interest containing the tumour, for Mouse #10, 12 and 8 respectively.

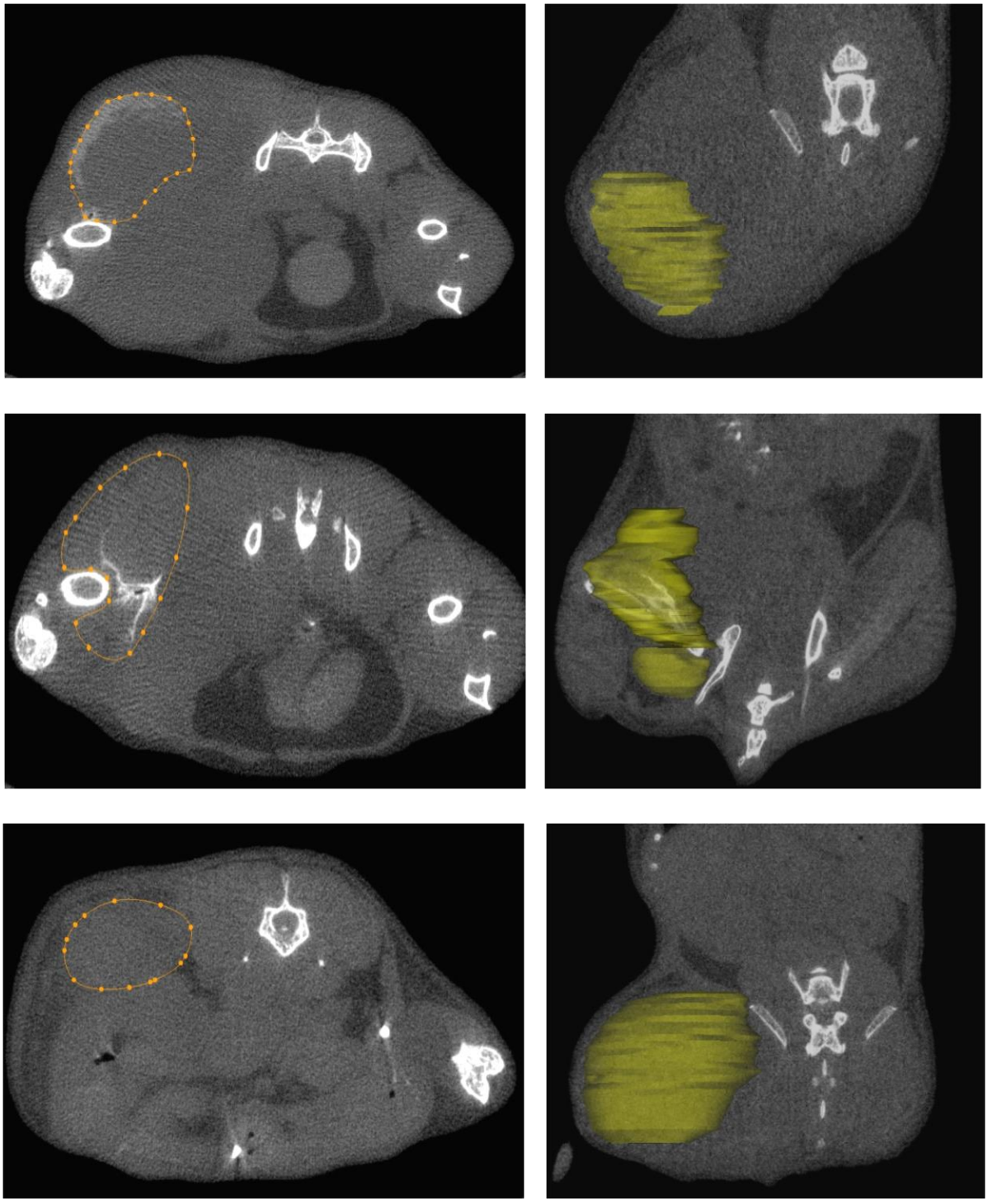

The specimen scans provided more favourable images when visualizing the contrast agent, as these were taken at a much higher resolution, ranging from 10-17.2 microns. The larger samples of mouse #4-6 were quite large and were therefore scanned at 17.2 microns. Figure 16 presents a sample of the specimen scans, using mouse #10 as an excellent example of contrast, mouse #12 as a moderate example, and mouse #8 as a less than favourable example. Due to the higher resolution used in specimen scanning as opposed to *in vivo* scanning, the contrast appears much more pronounced and well defined.

The OPT scans proved more challenging, and while the images did show fluorescence that appeared to correspond to the contrast seen in the micro-computed tomography scans, there was an abundance of background auto-fluorescence from the surrounding soft tissues. As is evident from Figure 16 using mouse #10, there appeared to be a fluorescent signal present from surrounding tissues that were not part of the tumour, and therefore not subjected to fluorescently-labeled gold nanoparticle contrast agent. We also viewed the OPT images using MicroView, and subjected the scans to isosurface rendering, similar to what was used for the micro-CT scans. This was done to register or co-localize the OPT and CT images, which indeed proved successful. While contrast may have been present in the OPT images, and co-localized to the micro-CT images, the abundance of background fluorescence and signalling, made it difficult to isolate the fluorescently-labeled gold nanoparticles.

Some of the tumors clearly were more aggressive with their growth reaching maximal levels much sooner than others. In addition, there appeared to be differences in the spread of the contrast agent between tumors. In some specimens, the contrast agent appeared to pool and show very little dispersion while in other tumors, it diffused well through the tumor and provided contrast to the periphery, allowing for differentiation between tumor and soft tissue.

The *in vivo* pre- and post-contrast scans, once registered, allowed for comparison and provided evidence that indeed contrast was present. With nothing other than contrast agent being introduced into the mouse between the scans, the resulting radiopacity present must have been the result of the injected gold nanoparticles. The benefit of using the specimen scanning is the increased level of resolution. By increasing the level of resolution of the scan, we effectively improve the spatial and contrast resolution, allowing for improved visualization and differentiation between the tumor and surrounding tissues.

Figure 14. Images of gold nanorods providing contrast for *in vivo* micro-CT scan at 50 microns resolution. Left image is pre-contrast and right image is post contrast injection of 20 µl of gold nanorod solution, of Mouse #10 (A), 12 (B) and 8 (C) respectively. Arrows point to tumour.

Figure 15. Image of 20 µl injection of gold nanorods providing for in vivo micro-CT scan of Mouse #10 (A), 12 (B), and 8 (C) respectively at 50 microns resolution. Left image is pre-contrast and right image is post-contrast (arrows point to tumour)

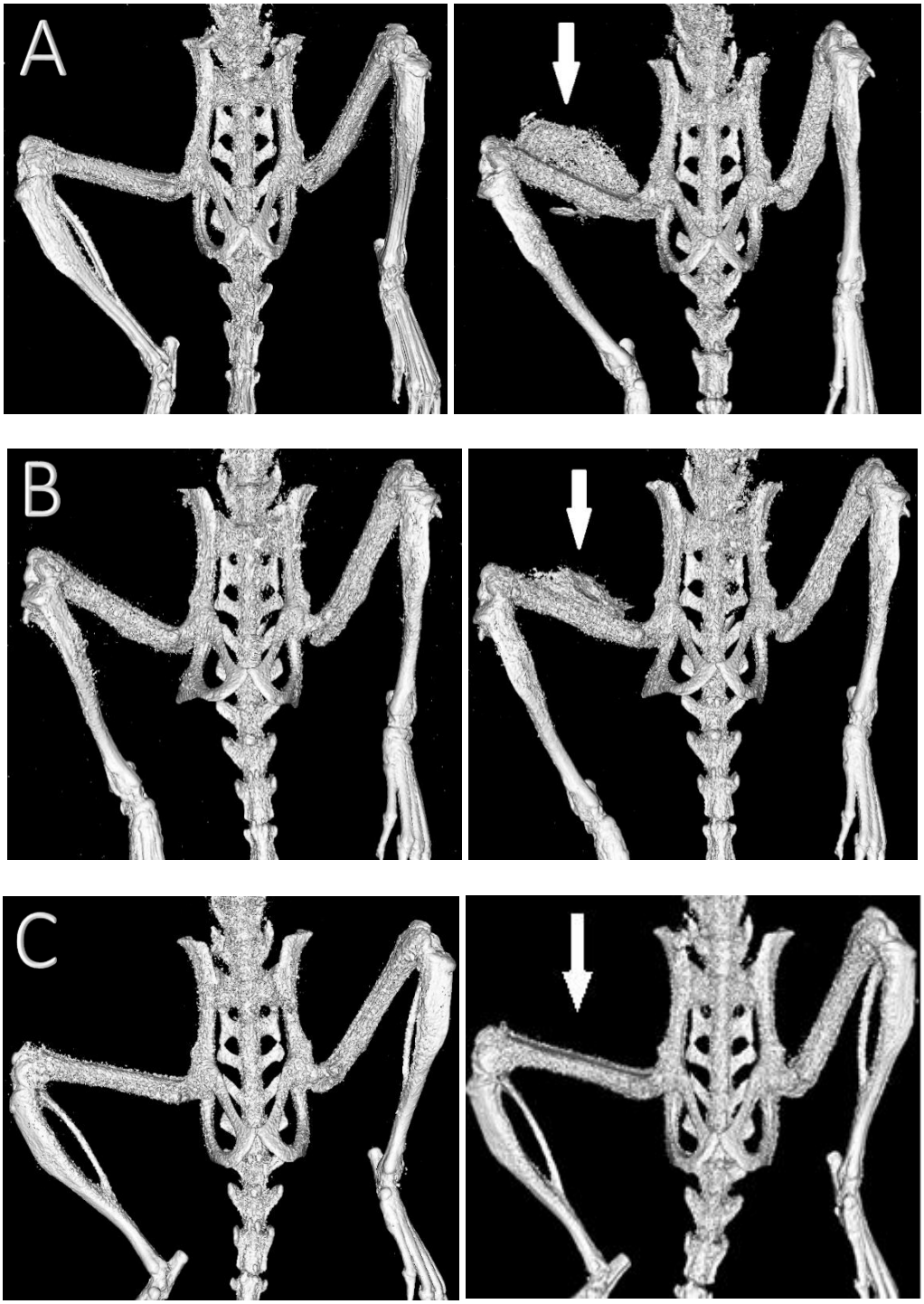

Figure 16. Image of tumour post-injection of 20 µl of gold nanorods providing contrast for specimen micro-CT scan at 10 microns resolution (LEFT), and OPT scan of dissected right hindleg (RIGHT). The sample was scanned at an exposure of 600ms, and UV light filter of TXR 560/40nm, 610nm used (RIGHT). Mouse #10 (A), 12 (B), and 8 (C) respectively. Arrows point to tumour.

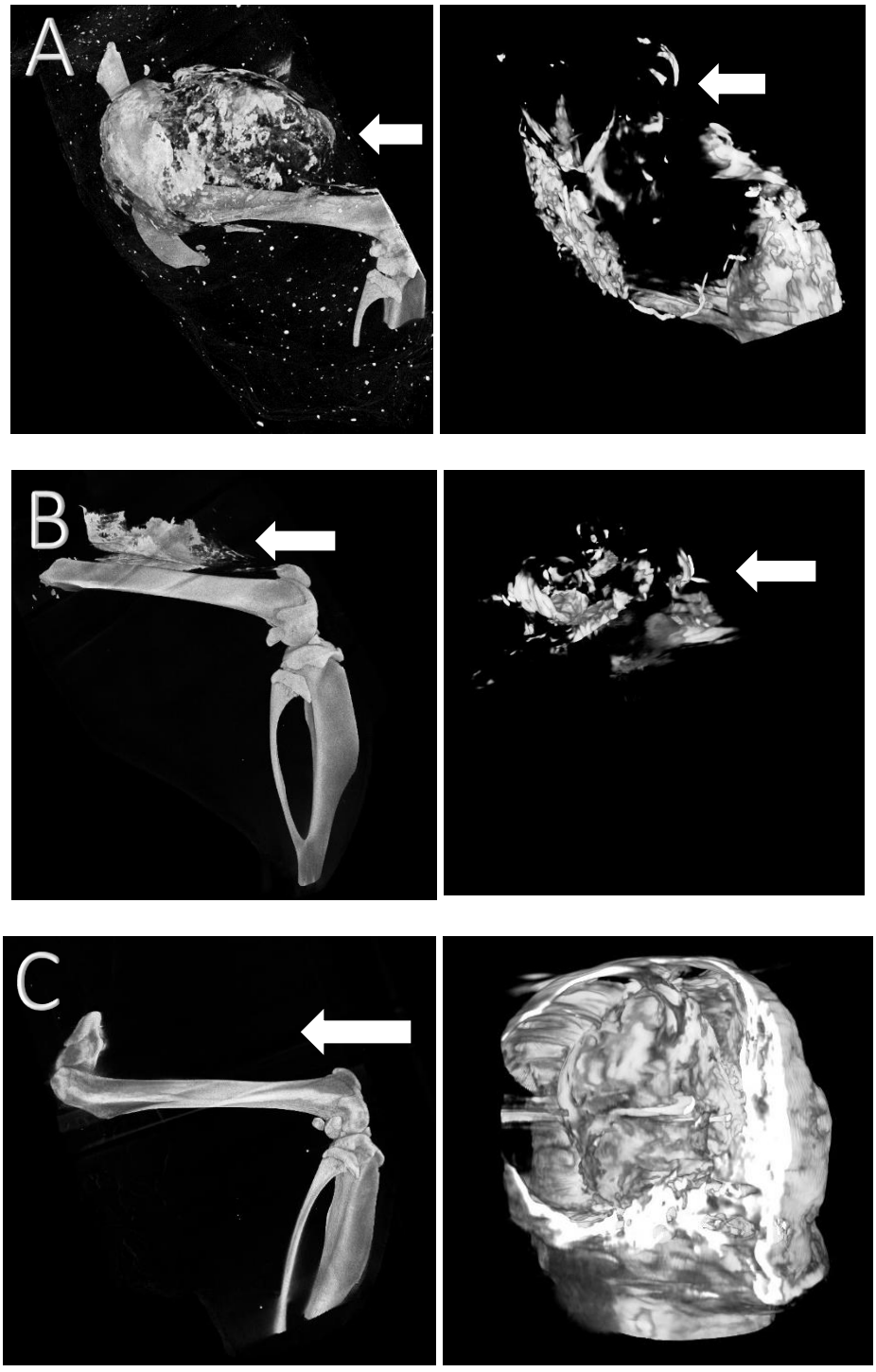

# Chapter 4: Discussion

## 4.1 Agarose Phantom

The fluorescently-labeled gold nanoparticles employed in this research project were intended for use in either 2D confocal or fluorescent microscopy. However, our experiment sought to answer the question as to whether or not they could be used for *in vivo* preclinical research. And if so, could they be visible under 3D micro-CT and OPT, and under what conditions.

The agarose phantom constructed, set out to answer these questions and to our delight, the Cy3-coated gold nanorods could not only be visualized under both imaging modalities, but their images could be co-localized (as evidenced from Figure 8). Several studies have looked at gold nanoparticles (both as spheres and rods) as an alternative to iodine as a preclinical contrast agent, and the attenuation reported has varied from 2.7 to 5.7 times that of iodine. (21,32) There are also studies that have assessed the contrast capability of gold nanoparticles as an *in vivo* contrast agent in mice specifically, and the results have been promising. (32) While it is known that gold nanoparticles can provide attenuation, and do so *in vivo*, very few studies have assessed the size of the gold nanoparticles and their affect on attenuation properties. Xu *et al.* used gold nanoparticles of varying size and concluded that the smaller the gold nanoparticle, the greater the x-ray attenuation. (33) While advantageous as a contrast agent, it is potentially toxic to the mice being studied at this size. (22)

It needs to be remembered that the fluorescently-labeled gold nanorods used were not meant for *in vivo* imaging. They were specifically designed for *ex vivo* research. The very fact that they could be seen under both imaging modalities is progress in and of itself. When the agarose phantom was constructed, only distilled water and agarose were used, in addition to the contrast agent. As was evident in the results section, only the contrast agent would have been able

to give a contrast signal in the micro-CT images, but also fluorescence in the OPT. This confirmed, that at least with respect to an agarose phantom, the Cy3 fluorescently-labeled gold nanorods could be seen. Having satisfied this requirement, the next step was to determine if the same fluorescently-labeled gold nanorods could be seen *in vivo* using mice.

## 4.2 *In Vivo* Systemic Injection

Our initial attempt to use the Cy3 fluorescently-labeled gold nanoparticles, systemically and intravenously, to compare and correlate the micro-CT scans with the OPT images, encountered difficulties. While the gold nanoparticles were visible in the agarose phantom testing, both for micro-CT and OPT, when the 50 OD and even the 250 OD gold nanoparticles were injected into the mice, the contrast could not be visualized on either modality. Even the AuroVist™ naked gold nanoparticles, which were reportedly already being used as an experimental micro-CT contrast agent, could not be seen on our scans. It is possible that the tail vein injections were unsuccessful however even if that was the case, we would have expected to see the gold pooled in the tail of these mice, which we did not. That suggests that the tail vein injections were successful, however the concentration of gold, once in the circulation, was not high enough to be seen. Clearly, the use of tail vein injections is a common practice in preclinical research and a multitude of studies show its effectiveness. (34–36) In fact, the use of an intravascular injection in the lateral tail vein is by far the most common technique employed for intravenous administration. (36) As was employed in our experiment, an insulin needle was used to inject the contrast agent as it is hubless, leading to less loss of the injected product. In addition, insulin needles can be obtained in gauge sizes of 28 and 29, making them ideal for tail vein injections. However, the direct method of tail vein injection employed also carries the disadvantage of it being difficult to see the blood flashback,

signalling successful entry into the tail vein. (36) The gold nanoparticles injected in our project were a very dark indigo colour which also made it nearly impossible to see any trace of blood flashback during injections. However, as alluded to, we would have expected to see the contrast pooled in the tail, even had we missed the vein. It was therefore concluded that the Cy3 fluorescently-labeled gold nanorods (both 50 OD and 250 OD) were not concentrated enough to be visualized as a contrast agent in micro-CT and OPT scans, when administered intravenously. Taking into consideration, that the entire blood volume was effectively diluting the concentration of gold nanoparticles, it was concluded that a much higher concentration would be required for intravascular contrast injection, or alternatively, to concentrate the contrast by providing a localized injection.

### 4.3 *In Vivo* Tumour Injection

An advantage to the use of gold nanoparticles as a pre-clinical contrast agent is that it allows for a single dosage of product, without the need for constant rate infusion. Depending on the size and shape of the particles, including the coatings or functional groups used, long circulation times are possible.(20) Additionally, gold as a whole is considered non-toxic and biocompatible, and as our research has shown, can be used to provide adequate contrast in micro-CT applications with small animals, when injected directly into tumours. (37) However, challenges remain in using fluorescently-labeled gold nanoparticles. As was mentioned previously, one challenge in the use of gold nanoparticles is in determining the concentration of particles needed to achieve adequate contrast, while not using more product than is necessary. In our project, we ran into issues with being able to standardize the size of the initial melanoma tumours. Other studies have looked at the growth rate and inevitable variability in the B16-F10

murine melanoma strain as well. It appears to be a common finding that the melanoma cells don't grow at the same rate in mice and can yield inconsistent results, with relatively large standard deviations in tumour volume. (38–40) Adding to the difficulties when working with live mice, being able to accurately measure an invasive tumour was more of a challenge than initially anticipated. While using calipers allows for a cursory measurement of the superficial portion of the tumour, it does not take into account the invasive nature of the murine melanoma strain used, and as was clearly evident, some of the initial tumours were very large as compared to latter ones. The issue was that these tumours were not standardized and therefore, injection of the contrast agent into the tumours may have yielded variable results based on that fact. Clearly, if a tumour was subjected to a higher relative concentration of gold nanoparticles, the resulting contrast should also be higher. It should also be remembered that the tumour volumes as presented in Table 5 and 6, were effectively estimates. The borders of the tumours were visualized and segmented using MicroView, but as should be expected, some liberties were taken to approximate the borders (it wasn't always clear where the tumour terminated, and muscle tissue began). As such, the generated volumes as shown in the tables, may not be accurate. However, in viewing the pre-contrast scans (as shown in Figure 14), the tumours could not be visualized at all, nor their borders estimated. So, while contrast wasn't always clearly apparent, there must have been some contrast present to allow for visualization of the tumour, post-injection of contrast agent.

By employing the isosurface feature present in MicroView, we were able to clearly identify the tumour periphery in several of the mice (see Figure 15). The oval or circular shape of the melanoma tumour is common in the early growth stages of soft tissue tumours and the contrast present correlated well with the higher resolution scans present in the specimen scanning portion of the project. A curious finding however was in the dispersion of the gold nanoparticles. Some

of the mice clearly showed a more uniform and rapid dispersion of contrast, while others seemed to pool and localize at the site of injection. Others still, showed no contrast in the *in vivo* micro-CT images yet under improved resolution with the specimen scanner, the contrast was clearly apparent. This was due to the nature of the specimen micro-CT scanner, in that the resolution offered is much higher than what the *in vivo* scans provide (10 microns vs 50 microns). The increase in resolution effectively improves the detail of the image and our ability to identify the nanoparticles. Lastly, in some of the mice, an obvious void or airspace was present where the needle puncture would have terminated and administered the gold nanoparticle contrast. Why this happened is unclear, but some interesting questions arise.

For our study, we injected the gold nanoparticles, waited 10 seconds, and in the time needed to close the hatch on the micro-CT machine and reintroduce the mouse into the scanner, the gold nanoparticles were allowed to disperse within the tumour. It is possible that if we would have allowed additional time between the injection and the scan, a more uniform dispersion of the nanoparticles may have been achieved. (25) Ideally, it would have been preferred if the gold nanoparticle contrast agent had had time to disperse evenly throughout the tumour and also to the periphery, to allow for differentiation between tumour border and surrounding soft tissues. Tumours, particularly benign, but also metastatic tumours in the early stages, are surrounded by a fibrous, connective tissue capsule that retains the tumour cells. (41,42) It is suggested that this capsule would potentially retain the gold nanoparticles as well. The question however, is how much time is required to allow for complete and uniform dispersion, which was beyond the scope of this thesis.

The main purpose of this project was to be able to correlate the images from micro-CT to the images obtained from OPT. By using a fluorescently-labeled contrast agent, the hope was that

additional preparation and/or staining would not be required to view the same contrast agent in OPT, as in micro-CT. By nature of the OPT machinery, if the specimens being viewed are quite large, it makes it physically difficult to both clear and prepare the samples for imaging, but also in retaining the sample to the mount while being scanned. The first challenge of clearing a dense, large sample can often be overcome with time, which we were successful with. The samples were given extended periods of time in both methanol and BABB and a level of clarity was achieved that proved satisfactory. The second aspect of sample size could not be overcome. In fact, we found that because the samples were so large (tumour and hindleg combined), they often dismounted from the OPT mid-scan and needed to be remounted and repeated. This also appeared to introduce movement artifacts in the scans which again affected the quality of the results. In addition, it appeared that the soft tissue surrounding the tumours (muscle tissue fibre) was providing an auto-fluorescence signal within the same wavelength range as the fluorescent label. Biogenic amines will react with formaldehyde to produce compounds with an emission maximum of 480 nm. (43) There have been reports of auto-fluorescence due specifically to the use of aldehydes as fixatives, with suggestions to reduce the auto-fluorescent signal by using a sodium borohydride bath after fixation, or by avoiding aldehyde fixatives altogether. (44) Alternative fixatives include those based on alcohols (mixtures of methanol, ethanol and propanol) or simply minimizing the percentage of aldehydes in the fixative agent itself. (45)

It is clearly apparent where the muscle tissues are as the striations can be seen with the naked eye, when imaging the OPT images of Mouse #10. In fact, reviewing Figure 16, comparing the micro-CT specimen scan and OPT of mouse #10, it is apparent that there is in fact co-localization between the two images with respect to contrast. However, there remains a considerable amount of background auto-fluorescence from the surrounding muscle tissue, and

possibly the melanoma tumour cells themselves. Mouse #10 proved most successful in being able to achieve co-localization, while the remaining mice proved more difficult.

While we were able to achieve co-localization between micro-CT and OPT imaging, it was clear that the auto-fluorescence of the muscle tissue and the melanoma cells themselves interfered with the interpretation of the results. (46) We successfully demonstrated that fluorescently-labeled gold nanoparticles can in fact be utilized as a contrast agent when attempting to visualize melanoma tumours in a murine model, under micro-CT, but consideration to possible changes to the gold nanoparticles or the tumour cells themselves, could be made. For example, it may be advantageous to consider using different fluorescent labels on the gold nanoparticles, which would allow for varying wavelength filters to be employed during the OPT scanning. Also, the use of a different tumour cell line may have also helped as our tumours were quite heavily pigmented and using a less pigmented cell line may have improved the results.

While questions remain as to the exact concentration that would be most effective in visualizing the tumour, including the timing required for complete dispersion of the gold nanoparticles, the proof of concept has been applied. These minor details could be addressed with future research projects. However, the hurdle associated with the auto-fluorescent nature of skeletal muscle tissue, in addition to the auto-fluorescence of melanoma cells themselves, would prove more challenging but nevertheless, should not be insurmountable. Consideration should be made in finding a fluorescent label that is in a far enough of a wavelength range as to not interfere with the auto-fluorescence we experienced. And with all that said, imaging of the tumours under micro-CT proved very successful and co-localization between the micro-CT images and the OPT images was indeed possible.

## 4.4 Targeted Delivery of Nanoparticles

The use of gold nanoparticles in different applications has been documented. In murine models, the *in vivo* targeted delivery of bisphosphonate-functionalized gold nanoparticles as contrast for detection of breast cancer calcifications was demonstrated. By using intramammary delivery, these gold nanoparticles allowed for CT visualization of the calcifications that would have otherwise gone unnoticed under standard mammography imaging. (47) Also relating to the field of oncology, there have been studies looking at the potential for early detection of cancer by employing molecular targeting of cells, that would be otherwise unseen in a standard CT scan. Popovtzer *et al.* demonstrated that using gold nanoparticles conjugated to UM-A9 antibodies, that the gold nanoparticles could accumulate in the targeted cells, at a rate 5 times higher than using non-targeted gold nanoparticles, or no contrast at all. (48) By utilizing the characteristic over-expression of transferrin on tumour cells, and specifically considering that it is the malignant phenotypes that most over-express it, gold nanoparticles could be used to target these cells specifically. (49) By targeting the transferrin over-expression (which is incidentally how conventional chemotherapeutics currently work) gold nanoparticles with an antibody to transferrin could be used to target and accumulate on these cancerous cells. This would not only allow for potential drug delivery systems to target tumour cells specifically, but new research in promising radiosensitizers suggests that the use of gold nanoparticles could allow for elevated radiation dose enhancement. (50) Hainfeld *et al.* have studied the effect of gold nanoparticles injected intravenously *in vivo* using mice with terminal intracerebral gliomas. After a period of 15 hours, the mice were imaged under CT and the tumours irradiated thereafter. The results found that the tumours had taken up the gold nanoparticles at a rate of 19:1 vs normal brain tissue, and that the resulting increase in irradiation dose was 300% higher, than in controls. Additionally, the mice

that received the gold nanoparticles in addition to irradiation of the tumours, had a 50% >1-year survival rate, compared to controls that had a 100% mortality rate. (51) Other researchers have conjugated gold nanoparticles to carbohydrates including glucose, mannose, and galactose, to target various tissues and study carbohydrate metabolic processes (52), while the conjugation of gold nanoparticles to TAT peptides (which are cell-penetrating peptides that facilitate the transfer of molecules across the cell), has also been studied, allowing specific delivery of pharmaceutical payloads in the study of HIV. (53) The possibilities appear endless as the ability to conjugate virtually any functional group, including fluorophores, to gold nanoparticles, plus their characteristic small size, makes them virtually perfect as a vector.

# Chapter 5: Conclusions and Future Directions

## 5.1 Conclusions

The use of a Cy3 fluorescently-labeled gold nanorod contrast agent, that could be visible under both micro-CT and OPT imaging, proved successful. From the results presented, the use of *in vivo* micro-CT imaging allowed for the gold nanoparticles to be visualized, while use of the specimen scanner allowed for a much better and higher resolution image, detailing exactly where the contrast agent was present. While OPT presented with its own set of challenges, the images did provide some level of fluorescence and we were able to co-localize the image with micro-CT. The novelty of this project was in the use of a Cy3 fluorescently-labeled gold nanoparticle, that was intended for 2D microscopy, and not 3D imaging. Being able to use this contrast agent and achieve the results we did, was rewarding. We were able to co-localize the images from both micro-CT and OPT, confirming that the contrast agent was visible and present in both imaging modalities.

Challenges included questions as to whether the concentration of contrast agent was adequate, and in the time required to adequately disperse the contrast agent within the tumour. As the size of the tumours were not standardized (initially, at least), possibly using a less aggressive tumour strain would have been more advantageous. In regard to the melanoma cell line used, it was heavily pigmented and may have affected the OPT results negatively. Lastly, the fluorophore used required a wavelength stimulation that also appeared to clash with the auto-fluorescence of the protein-rich muscle tissues. It may have been more appropriate to use a fluorophore that was far enough from the ultraviolet spectrum used, to better distinguish between the contrast and surrounding soft tissues. The auto-fluorescence of the muscle tissues also appeared to be related

to the use of formalin as a fixative, so substituting it with another alternative would be something to consider.

## 5.2 Future Directions

As we were able to visualize and co-localize the Cy3 fluorescently-labeled gold nanoparticles in both micro-CT and OPT, some refinement could be beneficial. Using a different fluorophore, along with less pigmented melanoma cells, and substituting the formalin with another product, could potentially improve results.

This study illustrates that gold nanoparticles can be fluorescently-labeled and viewed *in vivo* under micro-CT and OPT imaging. This characteristic allows for the tracking and tracing of the accumulation of the gold nanoparticles between two imaging modalities. By being able to identify and track the particles without the need for additional treatment of the samples, it would allow for fewer steps in processing, which would inherently minimize the risk of error.

As our study dealt with tumour visualization and size determination, the testing of tumour therapies could be assessed with conjugated gold nanoparticles, targeting the tumour cells. If a pharmaceutical company was attempting to assess the effectiveness of their latest cancer therapy, being able to visualize changes in tumour size, *in vivo*, without detrimental effects to the host, would clearly be advantageous. Many of these projects are staged and require extended monitoring, with animals being sacrificed at different time points. As gold nanoparticles can provide extended circulation times and bypass many of the issues with currently available iodine-based contrast agents, adding fluorescent-labeling would be an obvious improvement. Researchers could track the gold with multiple *in vivo* micro-CT imaging sessions, without the need to put the host at risk. This would also negate the need for multiple injections of contrast, and once having

reached experimental endpoint, the tumour sample could be visualized directly under OPT (and possibly microscopy), without additional staining.

## Bibliography


1. Kozomara S, Ford NL. Imaging of murine melanoma tumors using fluorescent gold nanoparticles. Med Imaging 2019 Biomed Appl Mol Struct Funct Imaging. 2019;10953.
2. Kagadis, George C, Ford NL, Karnabatidis DN, Loudos GK. Handbook of Small Animal Imaging: Preclinical Imaging, Therapy, and Applications. 1st ed. Karellas A, Thomadsen BR, editors. Boca Raton, FL: CRC Press, Taylor & Francis Group; 2016. 602 p.
3. DiMasi JA, Grabowski HG, Hansen RW. Innovation in the pharmaceutical industry: New estimates of R&D costs. J Health Econ. 2016;47:20–33.
4. Trachet E. Preclinical Success to Clinical Failure: Do We Have a Model Problem or an Endpoint Problem? [Internet]. [cited 2018 Nov 18]. p. 1. Available from: https://www.mibioresearch.com/knowledge-center/preclinical-success-clinical-failure-model-problem-endpoint-problem/
5. Li H, Zhang H, Tang Z, Hu G. Micro-computed tomography for small animal imaging: Technological details. Prog Nat Sci. 2008;18(5):513–21.
6. Sanjana P, Praveen B, Keerthi G, Shubhasini R, Shubha G. Comparison of gray values of cone-beam computed tomography with hounsfield units of multislice computed tomography: An in vitro study. Indian J Dent Res. 2017;28(1):66–70.
7. Pervova V, Lipengolts A, Cherepanov A, Abakumov M. Study of iodine, gadolinium and bismuth quantification possibility with micro-CT IVIS spectrumct *in vivo* imaging system. J Phys Conf Ser. 2017;784:1–4.
8. Choi HJ, Lee HJ, Kang SG. Computed Tomography - The Clinical Significance of Hounsfield Number of Metallic and Non-Metallic Foreign Bodies in the Soft Tissue. Soonchunhyang Med Sci. 2010;16(December):226–30.

9. O'Farrell AC, Shnyder SD, Marston G, Coletta PL, Gill JH. Non-invasive molecular imaging for preclinical cancer therapeutic development. Br J Pharmacol. 2013;169(4):719–35.

10. Lyons SK. Advances in imaging mouse tumour models *in vivo*. J Pathol. 2005;205(2):194–205.

11. Bouxsein ML. Guidelines for assessment of bone microstructure in rodents using micro-computed tomography. J bone Miner Res. 7AD;25(7):1468–86.

12. Detombe SA, Ford NL, Xiang F, Lu X, Feng Q, Drangova M. Longitudinal Follow-up of Cardiac Structure and Functional Changes in an Infarct Mouse Model Using Retrospectively Gated Micro-Computed Tomography. Invest Radiol. 2008;43(7):520–9.

13. Nebuloni L, Kuhn GA, Müller R. A Comparative Analysis of Water-Soluble and Blood-Pool Contrast Agents for invivo Vascular Imaging with Micro-CT. Acad Radiol. 2013;20(10):1247–55.

14. Ashton JR, West JL, Badea CT. *In vivo* small animal micro-CT using nanoparticle contrast agents. Front Pharmacol. 2015;6(Nov):1–22.

15. Diehl K, Hull R, Morton D, Pfister R, Rabemampianina Y, Smith D, et al. A Good Practice Guide to the Administration of Substances and Removal of Blood , Including Routes and Volumes. J Appl Toxicol. 2001;23(September 2000):15–23.

16. Cervenka L, Mitchell KD, Navar LG. Renal function in mice: effects of volume expansion and angiotensin II. J Am Soc Nephrol. 1999;10(12):2631–6.

17. Lin M, Marshall CT, Carolina N, Johnston SM, Carolina N. Quantitative blood flow measurements in the small animal cardiopulmonary system using digital subtraction angiography. Med Phys. 2009;36(11):5347–58.

18. Hallouard F, Anton N, Choquet P, Constantinesco A, Vandamme T. Iodinated blood pool contrast media for preclinical X-ray imaging applications - A review. Biomaterials. 2010;31(24):6249–68.

19. Willekens I, Lahoutte T, Buls N, Vanhove C, Deklerck R, Bossuyt A, et al. Time-Course of contrast enhancement in spleen and liver with exia 160, fenestra LC, and VC. Mol Imaging Biol. 2009;11(2):128–35.

20. Lusic H, Grinstaff MW. X - ray-Computed Tomography Contrast Agents. Chem Rev. 2013;113(3):1641–66.

21. Hainfeld JF, Slatkin DN, Focella TM, Smilowitz HM. Gold nanoparticles: A new X-ray contrast agent. Br J Radiol. 2006;79(939):248–53.

22. Chen YS, Hung YC, Liau I, Huang GS. Assessment of the *in vivo* toxicity of gold nanoparticles. Nanoscale Res Lett. 2009;4(8):858–64.

23. Pompa PP, Vecchio G, Galeone A, Brunetti V, Sabella S, Maiorano G, et al. *In Vivo* toxicity assessment of gold nanoparticles in Drosophila melanogaster. Nano Res. 2011;4(4):405–13.

24. Kinhikar RA, Tambe CM, Patil K, Mandavkar M, Deshpande DD, Gujjalanavar R, et al. Estimation of dose enhancement to soft tissue due to backscatter radiation near metal interfaces during head and neck radiothearpy - A phantom dosimetric study with radiochromic film. J Med Phys. 2014;39(1):40–3.

25. Maeda H, Wu J, Sawa T, Matsumura Y, Hori K. Tumor vascular permeability and the EPR effect in macromolecular therapeutics: A review. J Control Release. 2000;65(1–2):271–84.

26. Feeback D. Histology. 1st ed. New York: Springer-Verlag; 1987. 202 p.

27. Ancora D, Di Battista D, Giasafaki G, Psycharakis SE, Liapis E, Ripoll J, et al. Optical projection tomography via phase retrieval algorithms. Methods. 2018;136:81–9.

28. Nanopartz FAQz [Internet]. 2019 [cited 2019 Mar 20]. p. 1. Available from: https://www.nanopartz.com/faqz.asp

29. Ford NL, Mccaig L, Jeklin A, Lewis JF, Veldhuizen RAW, Holdsworth DW, et al. A respiratory-gated micro-CT comparison of respiratory patterns in free-breathing and mechanically ventilated rats. Physiol Rep. 2017;5:1–11.

30. Ford NL, Nikolov HN, Norley CJD, Thornton MM, Foster PJ, Drangova M, et al. Prospective respiratory-gated micro-CT of free breathing rodents. Med Phys. 2005;32(9):2888–98.

31. Faustino-Rocha A, Oliveira P, Pinho-Oliveira J, Teixeira-Guedes C, Soares-Maia R, da Costa R, et al. Estimation of rat mammary tumor volume using caliper and ultrasonography measurements. Lab Anim. 2013;42(6):217–24.

32. Kim D, Park S, Lee JH, Jeong YY, Jon S. Antibiofouling Polymer-Coated Gold Nanoparticles as a Contrast Agent for *in Vivo* X-ray Computed Tomography Imaging. J AM CHEM SOC. 2007;129(19):7661–5.

33. Xu C, Tung GA, Sun S. Size and Concentration Effect of Gold Nanoparticles on X-ray Attenuation As Measured on Computed Tomography. Chem Mater. 2008;20(13):2007–9.

34. Li S, Tang Z, Yu H, Li W, Jiang Y, Wang Y, et al. Administration of Naked Plasmid Encoding Hepatic Stimulator Substance by Hydrodynamic Tail Vein Injection Protects Mice from Hepatic Failure by Suppressing the Mitochondrial Permeability Transition. Jour Pharma Exp Thera. 2011;750–7.

35. Wang F, Nojima M, Inoue Y, Ohtomo K, Kiryu S. Assessment of MRI Contrast Agent

Kinetics via Retro-Orbital Injection in Mice : Comparison with Tail Vein Injection. PLoS One. 2015;10(6):1–11.

36. Vines DC, Mrt N, Green DE, Kudo G, Keller H. Evaluation of Mouse Tail-Vein Injections Both Qualitatively and Quantitatively on Small-Animal PET Tail Scans. J Nucl Med Technol. 2019;39(4):264–71.

37. Von Maltzahn G, Park JH, Agrawal A, Bandaru NK, Das SK, Sailor MJ, et al. Computationally guided photothermal tumor therapy using long-circulating gold nanorod antennas. Cancer Res. 2009;69(9):3892–900.

38. Foster WK, Ford NL, Med P, Holdsworth W, Foster WK, Ford NL. Investigating the effect of longitudinal micro-CT imaging on tumour growth in mice Investigating the effect of longitudinal micro-CT imaging on tumour growth in mice. Phys Med Biol. 2011;56:315–326.

39. Nguyen NN, Cornet A, Silvia B, Tabruyn SP, Foidart J, Noël A, et al. Inhibition of Tumor Growth and Metastasis Establishment by Adenovirus-mediated Gene Transfer Delivery of the Antiangiogenic Factor 16K hPRL. Mol Ther. 2007;15(12):2094–100.

40. Danciu C, Oprean C, Coricovac DE, Andreea C, Cimpean A, Radeke H, et al. Behaviour of four different B16 murine melanoma cell sublines : C57BL / 6J skin. Int J Exp Path. 2015;96:73–80.

41. Lodish H, Berk A, L ZS. Molecular Cell Biology. 4th ed. New York: WH Freeman; 2000.

42. Barr LC. The encapsulation of tumours. Clin Exp Metastasis. 1989;7(3):277–82.

43. Dodt HU, Leischner U, Schierloh A, Jährling N, Mauch CP, Deininger K, et al. Ultramicroscopy: Three-dimensional visualization of neuronal networks in the whole mouse brain. Nat Methods. 2007;4(4):331–6.

44. Beisker W, Dolbeare F, Gray JW. An improved immunocytochemical procedure for high-sensitivity detection of incorporated bromodeoxyuridine. Cytometry. 1987;8(2).

45. Tokumasu F, Dvorak J. Development and application of quantum dots for immunocytochemistry of human erythrocytes. J Microsc. 2003;211(June):256–61.

46. Dunn DR, Barth RF. Identification of melanoma cells by formaldehyde-induced fluorescence. Cancer. 1974;33(3):701–6.

47. Cole LE, Vargo-Gogola T, Roeder RK. Contrast-enhanced X-ray detection of breast microcalcifications in a murine model using targeted gold nanoparticles. ACS Nano. 2014;8(7):7486–96.

48. Popovtzer R, Agrawal A, Kotov NA, Popovtzer A, Balter J, Carey TE, et al. Targeted Gold Nanoparticles Enable Molecular CT Imaging of Cancer. Nano Lett. 2008;8(12):4593–6.

49. Schmidt J, Ryschich E, Huszty G, Knaebel HP, Hartel M, B MW. Transferrin receptor is a marker of malignant phenotype in human pancreatic cancer and in neuroendocrine carcinoma of the pancreas. Eur J Cancer. 2004;40:1418–22.

50. Botchway SW, Coulter JA, J CF. Nanoparticles For Diagnostic Imaging and Radiotherapy Special Feature : Review Article Imaging intracellular and systemic *in vivo* gold nanoparticles to enhance radiotherapy. Br J Radiol. 2015;88.

51. Hainfeld JF, Smilowitz HM, O'connor MJ, Dilmanian FA, Slatkin DN. Gold nanoparticle imaging and radiotherapy of brain tumors in mice. Nanomedicine. 2013;8(10):1601–9.

52. Fuente JM De, Penadés S. Glyconanoparticles : Types , synthesis and applications in glycoscience , biomedicine and material science. Biochim Biophys Acta. 2006;1760:636–51.

53. Fuente JM De, Berry CC. Tat Peptide as an Efficient Molecule To Translocate Gold Nanoparticles into the Cell Nucleus. 2005;1176–80.